Atmos. Meas. Tech. Discuss.,
doi:10.5194/amt-2019-81-RC1, 2019

Atmospheric Measurement Techniques Discussions

Interactive comment on "A Fast Visible Wavelength 3-D Radiative Transfer Procedure for NWP Visualization and Forward Modeling" *by* Steven Albers et al.

Anonymous Referee #1

Received and published: 20 June 2019

The manuscript presents a fast, approximate 3D radiative transfer procedure for visualization of numerical weather prediction and forward modeling of ground-, aircraft-, and satellite-based camera and imager. Reflection by optically thick cloud or aerosol layer is parameterized. The scattering phase function of cloud and aerosol is approximated by the double Henyey-Greenstein function. The model is capable of produce true-color images composed of radiances at three wavelengths in the visible spectrum. While the authors emphasized the usefulness of the model in data assimilation in weather models, future works are needed to actually apply to data assimilation. Technical details of the calculation method should be clarified. I believe that important improvements are needed in the manuscript. My recommendation is therefore to make major revisions.

Printer-friendly version

Discussion paper

Please find below my detailed comments.

General comments

1. A lot of technical details are missing. For example, a) authors mentioned about a combination of single and multiple scattering components of radiance and some interpolation method between optically thin and thick regimes, but the methods for the combination and interpolation are not given. b) Actually, what equations are used to calculate the total radiance? It is unclear how radiances are calculated when interactions between clouds and surface reflection is present. Please show equations of total radiance that accumulates all contributions from the atmosphere, clouds, aerosols, and surface. c) The method for determining "a single scattering phase function that is equivalent to the net effect of the multiple scattering events" is missing in the current manuscript. With unknown methods, I cannot judge the validity and values of the "approximations". I have raised more points in the "specific points" below.

2. This is probably because the technical details are obscured, I cannot evaluate the model's accuracy, validity and limitations. How accurate is this model? What approximations are used? These should be clearly stated in Abstract and Conclusions.

3. As indicated in Fig. 2, the model possibly uses the bidirectional (dual-path) ray tracing along lines of sight and paths from radiation source (i.e. typically the sun) to scattering points. However, actually, it is not clear how to compute the radiance. There is no description on evaluation of the integral of scattering contributions from segments of the line of sight. Or, maybe, the model does not actually compute the integral, but instead scattering contributions from aerosol and cloud elements are approximated to be from some single point within cloud or aerosol layer. Even if so, that "point" is unknown.

4. The adjoint of this radiative transfer model is not available, and more works are needed for data assimilation. I understand the adjoint is not necessary in some frameworks. However, this paper's focus is not data assimilation, anyway. Subsection 4.3

just suggests possibilities and outlook by lengthy descriptions lacking any evidence and results. I recommend to greatly shorten this part and merge into the last paragraph of Section 5.

5. Lens flare: Lens flare effects appear in actual total-sky images, which should be discussed if comparing the model simulations with camera images. The lens flare is significant in forward scattering directions and modify the appearance of solar aureole by aerosol particles. This is critical in determining aerosol properties from total-sky images.

6. Subsection 3.2 describes the optional characteristics of the model, which is interesting. However, it is not clear whether the authors are first presenting new modeling of this complicated modeling such as moonlight, city lights, and spherical atmosphere. Are there any previous papers regarding to things presented in this section? If so, the details should be found in those papers, and this paper should just cite the references. In the current form, the descriptions are too short to fully describe the complicated radiative sources such as city light, while no results of demonstration and verification are presented in this paper. If this section should be presented in this paper, supporting information including some examples of nighttime scene and Belt of Venus as the authors mentioned in the text. Anyway, this paper does not focus on such nighttime and twilight cases. I recommend to remove this subsection and to leave them for some separate papers. I hope to see example result, validation, and applications in the future.

Specific points

Title: Does the use of acronym of “NWP” conform to the regulation of AMT?

P1, L16: In my understanding, the proposed procedure is not intended for a radiation scheme in “weather and climate” models. The first paragraph of abstract loses focus.

P5, L20, “This is a unique feature that allows. . .”: The methodology is standard in the

field of atmospheric science, optics and computer vision. For example, MYSTIC, as used in Klinger et al. (2017), uses that standard method. The authors should give appropriate references.

P6: Eqs. (1) and (2) are identical, and there is no reason to present both.

P6, L6, Fig. 2 and Table 1: A method for radiance integration is not clear. In my understanding, the radiance should be an integral of contributions coming from many small segment of line of sight (from camera). Each contribution is a function of irradiance from radiative source, which should be calculated by the forward path using some spatial interpolation or directly tracing a ray from the scattering point to the radiative source. This kind of integration should be explained in detail. Without such a description, the readers cannot understand the relationship between forward and backward rays.

P6, L22, "615nm. . .": Please give a reason for selection of these 3 wavelengths. Is there any references?

P7, L1, "The light. . .": The same sentence is given previously.

P7: Eqs. (3) and (4) are identical, and there is no reason to present both.

P9, L4, "A two-stream approach is used to incorporate the backscatter fraction. . .": This sentence is not clear. There are several two-stream approaches. References should be given. Or, is this paper presenting a new two-stream approach for rendering? The definition of backscatter fraction should be clarified. How is the backward fraction used to determine the total downward illumination? What is "illumination"? Is it equal to the irradiance?

P9, L24: Why are HG functions used? Why not Mie theory? The reason should be explained in the text.

P10, Eq. (6): Explanations of i and theta are missing.

P10, Eq. (7): An explanation of ci is missing.

P10, L4: “When $\tau \ll 1$”: Please give an exact definition of tau. In Eq. (2), tau is optical depth integrated along the beam path. The definition of “beam path” is not clear because there are two paths: from camera to target and from the sun to target. In Eq. (8), how is tau defined? Is it the optical thickness along line of sight, along the direct source beam, or some combination of them? For volumetric object (i.e. cloud), there are infinite number of forward paths (from sun) corresponding to small path segments along the backward path (from camera).

P10, L15-17, “more efficient approximation that arrives at a single scattering phase function...”: This approximated phase function is not given in Subsubsection 3.4.2. I also failed to find any description in the manuscript. I guess the phase function should be modified to represent multiple scattering effects. How are they modified from the original single-scattering phase function?

P10, L17-18: The interpolation scheme is not actually given in Subsubsection 3.4.2. I also failed to find any details of this interpolation in the manuscript. What interpolation scheme is actually used between optically thin and thick clouds? Please show it using equations if possible.

P10, L26: Does “heavy overcast sky” mean sky with 100% cloud cover? How is the radiance parameterized as a function of cloud cover? How is the radiance computed when the sky is not overcast?

P11, L7, “Intermediate values of tau_0 are given empirical phase functions”: How are tau_0 and the empirical phase functions related?

P11, L28, “A simple bidirectional. . .”: How is the BRDF developed? Is it based on any measurements or theoretical calculations using rigorous radiative transfer models? It is better to show equations of the ARF.

P12, L9: Actually, what and how is interpolated? Is the cloud albedo (or BRDF) interpolated? Is it linear interpolation with respect to tau? It is better to explain the method

with equations and references (if present).

P13, L25: This paragraph mentioned about single-scattering albedo (for single scattering radiance), but previous explanations say that scattering contributions by aerosols do not depend on the single-scattering albedo (Eq. (8)). In P10, L7, single-scattering radiance is insensitive to the single-scattering albedo: “This relationship applies to hydrometeors as well as aerosols”. If so, why single-scattering albedo is discussed in P13.

P14, L6, “The first row in Table 2 was derived semiÂ■empirically for relatively dusty days”: How was the camera radiometrically calibrated? Were all pixels of camera image used? Was the circumsolar region excluded or obscured by shadow band or anything? Of course, saturated pixels should be excluded. Are there any references?

P14, L11, “AERONET”: References are needed.

P15, L3-7, “As with cloud multiple scattering, a rigorous approach such as MonteÂ■-Carlo would consider each scattering event explicitly, though this would be computationally inefficient. . . . multiple scattering events.”: These 2 sentences are almost identical as previously shown in the hydrometeor subsection. Please make a point clear.

P15, L10 and L21, “eq. 6”: The equation number seems wrong.

P15, L11: What are CIRA, RAMS, and WRF? They are explained at page 18, but it is too late. Also, references are needed.

P16, L6, “these quantities are merged together to provide the combined radiance”: How are they merged? Is the combination simply a sum of radiance components by clear sky and aerosol/cloud? How does the model implement the transmissivities between the sun and cloud/aerosol and between the cloud/aerosol and the camera? Please show equations if possible.

P17, L2-5: A lot of details and references are missing. What is “relatively simple an-

alytical function"? How is the f "modified"? What a sun glint model is chosen from many previously proposed models? How is "scattering from below the water surface" modeled? If there are references, please cite them. If there is no reference, described the details.

P18, L3, "3x3 transfer matrix": Please provide this matrix explicitly or show a reference. This is because there are several variants of RGB color space.

P19, L2, "A more complete. . .": This sentence is not clear. Is this confirmed by tests or just a guess by the authors? Is there any evidence?

P18, L31, "we've" → "we have"

P18, L31: "Simulated Weather Imagery (SWIm)" → "SWIm" (This is already written at P4, L7 and should not be repeated)

P20, L23, "Local Analysis and Prediction System Â■ LAPS, Toth et al., 2014)" This should be presented earlier because LAPS appears at P19, L9.

P20, L25, "METAR": What is METAR?

P21, L8, "High Resolution Rapid Refresh (HRRR)" → "HRRR". HRRR first appeared earlier. It should be explained when presented first.

P21, Subsubsection 4.2.1: In this comparison of simulated observed imagery, strong direct sun beam can cause lens flare, which should be taken into account. The lens flare may be significant particularly when strong direct beam is incident to the camera as in Fig. 11. The camera image cannot be directly compared with the simulated image.

P21, L26, "The brightness scaling...": This should be primarily influenced by the lens flare.

P22, L7, "GFS": What is GFS?

P22, L17, “uncertainty in the brightness scaling of the DSCOVR imagery” : Why is it uncertain? If the radiance data are from the EPIC product, the brightness scaling should be the same as for simulated imagery.

P23, L32, “One approach would entail developing SWIM’s Jacobian or adjoint, while other techniques employ recursive minimization.”: This sentence is not clear. Please give references. The authors stated that “SWIm can be used as a forward operator in a variational minimization”. However, the derivatives are required in the variational minimization, while derivative calculations are not in scope of the current manuscript. This is confusing. It is not very clear whether he current SWIM be used for data assimilations or further works are needed.

P23, Subsection 4.3: This section seems to be the authors’ outlook. The problem is that it is not clear whether it is outlook or not. It is better to shorten this part and move to Section 5.

P24, L1: There are no references of GSI, Joint Environment for Data Integration (JEDI), variational LAPS (vLAPS).

P24, L9, “We are. . .”: This paragraph briefly presents an ongoing work without any evidence, results, and detailed explanations. I recommend to delete this paragraph and leave it for future papers.

P25, L18, “to assimilate observed imagery via a comparison of such with simulated imagery produced by SWIM from first guess NWP forecasts” : In my understanding, the current SWIM cannot be used for data assimilation, and the improvement is left for future works. This sentence is wrong, or it is just the authors’ outlook.

P25, L33-: This and subsequent paragraphs mainly describes the author’s outlook, using more spaces than pure conclusions of this paper. I think the authors have too much emphasis on the outlook.

Figure 1 presents a copy from a paper. Does this conform to the copyright? Is there no

problem to reuse the copy of the figure of Klinger et al. (2017)?

Figure 1 summarize few selected radiative transfer models, while there are significantly more 1D and 3D models over the world. The objectives of them are very different, and the purpose of presentation of this figure is not clear. It should be clarified how the models are selected. For example, are they candidates used for data assimilation in NWP, or can they all produce color imagery?

The table in Fig. 1 should be separated and presented as a table (not in a figure).

Figure 2, "...and used for subsequent calculations to estimate the radiance": tau_s should vary by location on the line of sight. How is the radiance actually calculated using tau_s and tau_o? The details should be explained in the main text possibly with equations.

Interactive comment on Atmos. Meas. Tech. Discuss., doi:10.5194/amt-2019-81, 2019.

Printer-friendly version

Discussion paper

Atmos. Meas. Tech. Discuss.,
doi:10.5194/amt-2019-81-RC2, 2019

Atmospheric Measurement Techniques Discussions

Interactive comment on "A Fast Visible Wavelength 3-D Radiative Transfer Procedure for NWP Visualization and Forward Modeling" *by* Steven Albers et al.

Anonymous Referee #2

Received and published: 5 August 2019

The manuscript describes an exciting visualization tool that allows comparison between output of numerical weather forecast models and camera or satellite observations. I congratulate the authors to this development! The manuscript is therefore an important contribution within the scope of the journal. However, I have major concerns about the manuscript, which need to be addressed before publication. In particular I am concerned about the frequent reference to data assimilation. For that purpose, the uncertainty of the method needs to be characterized quantitatively which hasn't been done at all. At least it is not obvious from the manuscript. My major points are, in some more detail:

Printer-friendly version

Discussion paper

- Description of several methods is missing, most important multiple scattering by clouds and aerosol; I was expecting some more details concerning the methods, in particular how those are applied in 3D geometry. In particular, aerosol and cloud layers observed from above are described, but I didn't find enough information about how the calculation from below and from the side is done.
- A quantitative validation of the method is missing. A number of pictures is provided which show a visual comparison of model results with camera images or satellite observations. One could infer that the model "obviously" works since the comparison looks realistic. But this type of comparison includes uncertainties of the radiation operator and differences between real situation and NWP model output; in particular for data assimilation a more quantitative characterisation of the uncertainty of the operator is required, e.g. by comparison of SWIm with independent model results.
- The manuscript contains a number of unproven claims which need to be proven in the manuscript or a reference needs to be provided; I'll give a number of examples in the specific points below.

Carefully addressing these points is critical in order to reach the scientific quality and presentation quality required for publication in AMT. To consider the second point, it would be possible to phrase the applicability to data assimilation more carefully (and to phrase it less often). Even then, however, at least some comparisons with an accurate 1D radiative transfer model are strongly suggested, which should not be that difficult.

Specific points:

Page 5, line 32: "can be benchmarked" - if so, why hasn't at least some benchmarking been done?

Page 5, line 35: Some more detail and explanation is required: I am not sure how you do this forward-backward calculation. Isn't that like a typical single scattering approach,

following the radiation from the source to the detector or the other way round?

Page 7, line 18: "integrated ... weighted by the cosine of the zenith angle"

Page 7, line 21: This is one of the above mentioned unproven claims, "the resulting radiance is nearly proportional to the spectral radiance at 540nm". Please demonstrate or provide reference!

Page 7, line 31: What you propose here is very similar to the relationship between PAR (photosynthetically active radiation) and GHI, and there is a number of references in the literature studying this relationship.

Page 8, line 7: How did you come up with these decisions/numbers?

Page 9, line 4: Please more specific! What kind of two-stream? You are interested in the radiance and thus the angular distribution - how do you handle that with the twostream? How do you apply the twostream in 3D, if you look sideways at a cloud?

Page 9, line 11: With hydrometeor density you mean the density of liquid water or ice?

Page 9, line 18: Bilinear in 3D space?

Page 9, line 24: What kind of "combination"? One in the forward and one in the backward direction, as in Key et al, Parameterization of shortwave ice cloud optical properties for various particle habits, JGR 2002?

Page 9, line 24: Why is the Henyey-Greenstein approximation needed? Couldn't you use the real phase function? Later in the text (page 21), it is stated that "SWIm was tested and can realistically reproduce rainbows, twilight sky colors and other atmospheric phenomena (Albers and Toth, 2018)." which is only possible with the real phase function but certainly not with Heyne-Greenstein.

Page 10, line 27: For an optically thick cloud one would expect (1 + 2 mu)/3 (old literature on asymptotic theory, and easily confirmed with a 1D radiative model). Here it is 1 + 4mu)/3 - how did you come up with this equation?

Page 11, line 15: The backscatter fraction is extremely important in this context - please explain in more detail and give the equations.

Page 12, line 6: Is that true? With increasing polar angle z0 the reflectance should become larger since the path length through the medium becomes longer.

Page 12, line 12: The history is not relevant here

Page 12, line 16: Faster than what?

Page 12, line 27: Equation 10 and 11 show two different expression for the double-Henyey-Greenstein function. My understanding of the DHG was more like equation 11. Which one do you use?

Page 14, line 7: Please explain in more detail what semi-empirical means in that context.

Page 16, line 5: What does that mean? Doesn't the model grid cover the whole atmosphere?

Page 17, line 3: What relatively simple functions?

Page 17, line 6: There is a well-established model of ocean BRDF by Cox and Munk, 1954. Do you use that or do you do something similar / completely different?

Page 17, line 21: I was a bit surprised that you first selected three wavelengths according to the colors RGB. Why not directly use the three wavelengths as input to the matrix? Does it make a noticable difference if the three computational wavelengths were used directly as RGB or if the described interpolation preocedure is applied?

Page 20, line 1: Validation of SWIm itself is missing (see major point above)

Page 20, line 17: As far as I understood, the method is not yet ready and the uncertainty hasn't been quantified.

Page 23, line 32: You don't have an adjoint yet, do you? Is the adjoint easily developed?

Figures are not in ascending order. E.g. Figure 9 is referenced in the text before Figure 6.

Interactive comment on Atmos. Meas. Tech. Discuss., doi:10.5194/amt-2019-81, 2019.

Printer-friendly version

Discussion paper

Reviewer #1

General Comments:
---

1. More details on the forward light rays and 3D irradiance field are now discussed in Section 3.4.

a) the method of interpolating between the single & multiple scattering cases is now given in section 3.4.2

b) The final combination of clear and cloudy contributions to the radiance is now specified in section 3.6, with the individual steps described in earlier sections. Surface albedo is discussed in section 3.7.

c) the procedure for handling multiple scattering with an effective single scattering phase function was elaborated upon for cloud liquid. Similar formulations (not shown) are used for cloud ice, rain and snow.

2. Additional equations have been added in various sections to more completely describe the total (and solar relative) radiance. The overall accuracy of SWIm is now summarized in Table 4, and the items within this table are discussed in the conclusion and elsewhere in the manuscript.

3. Computation of radiance is now given in greater detail throughout the manuscript (e.g. section 3.4.1).

4. We believe section 4.3 gives a useful review of related 3D assimilation methods that include the use of visible light wavelengths and cameras. We now provide some results (Figure 14) that illustrate preliminary steps we are taking to develop a SWIm based assimilation. We agree there is much more to be done.

5. Lens flare is now mentioned in a more general context at the end of section 4.2.3.

6. Details on moonlight, city lights, and spherical atmosphere will be deferred to a future paper and this has been clarified in the text.

Specific points

Title: "NWP" is now spelled out

P1, L16: The first paragraph of the abstract provides context about the importance of visible wavelength radiation in modeling and we believe the 3rd paragraph of the abstract discusses the more focused role of SWIm in a reasonable manner.

P5, L20: The last paragraph of section 2 along with parts of section 3.8 have been modified to reflect the reviewer's suggestions.

P6, Eqs. (1) and (2) are indeed identical. We now only show the second equation.

P6, L6: The method for radiance integration, with Step 2 (clear sky) ray tracing as an example, is now shown in Eq. 3.

P6, L22: The rationale for wavelength selection was elaborated upon.

P7, L1: The redundant sentence was removed

P7, Eqs. (3) and (4) are indeed identical. We now only show the second equation.

P9, L4: This line and section has been revised to improve clarity. "Two-stream" isn't mentioned now since we use a different relatively simple approach. "Illumination" has also been replaced by "irradiance" in this section.

P9, L24: Rationale for using HG functions is now given in sections 3.4.1 and 3.4.2

P10, Eq 6: Definitions of i and theta are now in place

P10, Eq 7: c(i) was changed to f(i) and is now defined as a summation

P10, L4: Tau is now more clearly defined in this context

P10, L15-17, 17-18: The phase function is now more completely described for the case of cloud liquid, though the formulation isn't yet detailed for cloud ice, rain, or snow.

P10 L26: In the context of this section, "heavy overcast" means the 3D irradiance field (eq. 8) at the location of the portions of the cloud along the line of sight closest to the observer is ~<0.4. This definition of overcast is independent of cloud fraction and related quantities.

P11 L7: The intermediate phase functions are now described in section 3.4.2.
P11 L28: A simple ARF parameterization was developed with references and equations now given in section 3.4.3.

P12, L9: It is now stated that linear interpolation with respect to cloud albedo is used to approximate the reflectance between the low τ and high τ regimes.

P13 L25: Single scattering albedo is now included in eq. 11 since this is considered for aerosols with the single scattering radiance calculation.

P14, L6: The items mentioned by the reviewer are now clarified in the text within section 3.5.2.

P 14, L11: An AERONET reference was added in section 3.5.2.

P15, L3-7: These two sentences are now condensed for clarity and to avoid repetition.

P15, L11: These chemistry models are now better explained here, including references.

P16, L6: More details and equations are now given in section 3.6.

P17, L2-5: A reference was added that we base the ocean reflectance upon. Brief descriptions are given for the handling of land anisotropic reflectance.

P18, L3: The transfer matrix is now explicitly supplied

P18, L31: Wording adjusted to follow both suggestions

P19, L2: "A more complete" appears in the text on P18, L25. A more specific reference to Rayleigh correction is being added for the satellite example. For everyday photography this is more of a general comment that images often have more saturation, or may suppress the atmospheric brightness with polarizing filters and the like, all for the purpose of making the image look more appealing.

P20, L23: The LAPS reference was moved to section 4.1 and the LAPS description was clarified in section 4.2.

P20, L25: A more general description is now used for the METAR observations

P21, L8: The HRRR acronym is now expanded upon its first use.

P21, sec 4.2.1: We agree and lens flare is now mentioned there in the text.

P21, L26: In a camera image, the regions that are saturated (hence not useful for quantitative brightness comparison) can reach that brightness from either lens flare or sunlight scattering by aerosols and clouds, depending on the situation and quality of the camera. A clarifying sentence was added here.

P22, L7: GFS is now defined

P22, L17: The strategy for producing figure 12 is now explained in more detail to address the reviewer questions, within section 4.2.2.

P23, L32: We state that "One approach would entail developing SWIm's Jacobian or adjoint". This should clearly imply that it has yet to be done.

P24, L1: References for vLAPS, GSI were added. JEDI is now referenced with a website since this appears to be unpublished at this time.

P25, L18: The revised text now describes a simple camera assimilation technique we performed that can serve as an introduction to the other methods mentioned in our roadmap.

P25, L33: As now mentioned in the last paragraph of Section 1, this study is intended to introduce SWIm, and describe what has been done so far, and suggest a roadmap for the future.

Figure 1: We are no longer using the image from another paper. This has now been converted into Table 1. The table is intended to show a variety of RT packages and for context to illustrate which ones have similar capabilities as SWIm. The other questions are now addressed in section 2 of the text.

Figure 2: Section 3.3 now has an equation illustrating how radiance is computed as an integral from the rays traced in the figure. In this section, the simple example of Rayleigh or Mie single scattering is illustrated. Additional equations relating to multiple scattering are given in section 3.4.

Reviewer #2

General Comments:

The authors are glad the reviewer appreciates the relevance and value of SWIm. We appreciate the major concerns and would like to respond both generally and specifically. Data assimilation is now mentioned mainly in the context of future work. However even with significant approximations in the radiative transfer it is possible to perform simple types of assimilation with metrics like the correlation coefficient as now described in the text. Evaluation of the 1D radiative transfer has been performed in the context of the distribution of reflectance values at the red wavelength in DSCOVR / EPIC imagery for both clear and cloudy regions. Oceanic clear areas are in the expected range of 5-6% reflectance factor with the bright tops of tropical convective clouds between 1.0 and 1.1.

Specific points

P 5, L32: As now discussed in Section 5, specific comparisons with other radiative transfer packages (e.g. CRTM, MYSTIC) is a good topic for future work. Thus far we've focused mainly on comparisons with ground-based cameras, pyranometers, and DSCOVR imagery, even though they typically include the LAPS cloud analysis used for SWIm input in the evaluation pipeline.

P 5, L35: The forward-backward ray-tracing procedure has now been clarified in section 3 of the text.

P 7, L18: The zenith angle weighting is now mentioned in the text.

P 7, L21: A simple calculation of this was performed and now summarized in the last paragraph of section 3.1.

P 7, L31: We would like to investigate this further in the literature and report in a followup paper. Thus far the authors have only seen information about this in the form of an online solar spectrum calculator used within the solar power industry.

P 8, L 7: The statements about the moon's brightness came from a literature search about the "opposition effect". It is now made clear in the manuscript that details about the moon's brightness will be deferred to a future paper.

P 9, L 4: The "two-stream" term was used too loosely and the description has now been updated to make the detailed procedure more clear.

P 9, L11: The density is based on the hydrometeor type and the effective radius as now mentioned in the text.

P 9, L18: “bilinear” is now replaced with “trilinear” since light rays are traced in 3D space.

P9, L24: The linear combination of HG functions is now introduced in section 3.4.1 and further described in section 3.4.2 and Appendix B. The HG function terms provide for both forward and backward scattering.

P9, L24: Rationale for using HG functions is now given in sections 3.4.1 and 3.4.2, particularly with the convenience of being able to raise “g” to an exponent to approximate multiple scattering.

P 10, L 27: This was chosen empirically, partly since it averages to 1 with respect to zenith angle. We will try your formulation since it will probably help improve the pyranometer comparisons with overcast conditions, camera image comparisons with partly cloudy conditions, and have better theoretical footing as you suggest.

P11, L15: The procedure for calculating the backscatter fraction is now given in section 3.4.3.

P12, L6: We would suggest the increasing optical path of the sunlight through optically thin cloud or aerosols shouldn’t affect the observed radiance (technically the reflectance factor), since we are in a single scattering regime. The path length from the observer through the medium is remaining constant.

P12, L12: The HAALE-MURI history has been removed, while this project is represented in the Acknowledgements section.

P12, L16: 1-D aerosol calculations are faster than 3-D aerosols as now clarified in the text.

P12, L27: Eq. 11 represents a pair of DHG functions from eq. 10 as now explained further in the text.

P14, L7: The semi-empirical procedure is now explained in more detail in the text.

P16, L5: SWIm is designed to work even in cases when the NWP grid is limited in horizontal or vertical extent. This helps save computing resources and allows SWIm to work with limitations in NWP systems.

P17, L3: A reference was added that we base the ocean reflectance upon - this is the same one the reviewer suggested.

P17, L6: A reference was added that we base the ocean reflectance upon. Brief descriptions are given for the handling of land anisotropic reflectance.

P17, L21: The Bell et al. reference describes some experiments that help show the value of having a more complete spectrum to get the best chromaticities and color rendering. The interpolation procedure we describe will by design produce a more accurate spectrum and hence chromaticity, compared with simply inserting three narrowband wavelengths into the CIE color matching functions. We also in the text now give the rationale for selecting the three reference wavelengths used within SWIm.

P20, L1: In addition to image correlation, subjective evaluation of the 1D radiative transfer has been performed in the context of the distribution of reflectance values at the red wavelength in DSCOVR / EPIC imagery for both clear and cloudy regions. Ground-based comparisons of global horizontal irradiance (GHI) have also been done. A more rigorous comparison of SWIm with another 3D radiative transfer model (e.g. MYSTIC, SHDOM) is planned for a future paper..

P20, L17: The solar irradiance (GHI) comparisons are now being done with case studies of clear and partly cloudy conditions (e.g. section 3.1 - Fig. 2, section 4.2.1 - Figs 2,10), and overcast skies though not yet in a more systematic manner.

P23, L32: We have clarified in the text that the adjoint has yet to be developed. We think it is feasible to do in the future. Minimization methods that do not require an adjoint would also be possible.

A Fast Visible Wavelength 3-D Radiative Transfer ~~Procedure for NWP~~Model for Numerical Weather Prediction Visualization and Forward Modeling

Steven Albers[1], Stephen M. Saleeby[2], Sonia Kreidenweis[2], Qijing Bian[2], Peng Xian[3], Zoltan Toth[4], Ravan Ahmadov[5,4], Eric James[5,4], and Steven D. Miller[2]

1 - Spire Global, Inc., Boulder, CO
2 - Colorado State University, Ft. Collins, CO
3 - U.S. Naval Research Laboratory, Monterey, CA
4 - Global Systems Division, ESRL/OAR/NOAA,
5 - CIRES at Global Systems Division, ESRL/OAR/NOAA

Abstract:

Solar radiation is the ultimate source of energy ~~for~~flowing through the atmosphere fueling all atmospheric motions. The visible wavelength range of solar radiation represents a significant contribution to the Earth's energy budget and visible light is a vital indicator for the composition and thermodynamic processes of the atmosphere from the smallest weather to the largest climate scales. The accurate and fast description of light propagation in the atmosphere and its lower boundary environment is therefore of critical importance for the simulation and prediction of weather and climate.

Simulated Weather Imagery (SWIm) is a new, fast and physically based visible wavelength 3-dimensional radiative transfer model. Given the location and intensity of the sources of light (natural or artificial) and the composition (e.g., clear or turbid air with aerosols, liquid or ice clouds, and precipitating rain, snow, or ice hydrometeors) of the atmosphere, it describes the propagation of light and produces visually and physically realistic hemispheric or 360° spherical panoramic color images of the atmosphere and the underlying terrain from any specified vantage point either on or above the Earth's surface.

Applications of SWIm include the visualization of atmospheric and land surface conditions simulated or forecast by numerical weather or climate analysis and prediction systems for either scientific or lay audiences. Simulated SWim imagery can also be generated for and compared with observed camera images to (i) assess the fidelity, and (ii) ~~and~~ improve the performance of numerical atmospheric and land surface models, as well as ~~(iii) through their inclusion into an observational~~through the use of the latter in a data assimilation scheme, (iii) improve the estimate of the state of atmospheric and land

surface initial conditions for situational awareness and NWP forecast initialization ~~applications~~purposes.

1. Introduction and Motivation

Numerical Weather Prediction (NWP) modeling is a maturing technology for the monitoring and prediction of weather and climate conditions on a wide continuum of timescales (e.g., Kalnay 2003). In NWP models, the large scale variability of the atmosphere is represented via carefully chosen and geographically systematically laid out prognostic variables such as vertically stacked latitude/longitude grids of surface pressure, temperature, wind, humidity, suspended (clouds) and falling (precipitating) hydrometeors, aerosol, etc. Using differential equations, NWP models capture temporal relationships among the atmospheric variables, allowing for the projection of the state of the atmosphere into the future. Short range NWP forecasts (called "first guess") can then be combined with the latest observations of atmospheric conditions to estimate the instantaneous weather conditions at any point in time (called analyzed state, analysis, or forecast initial condition), using Data Assimilation methods (DA, e.g. Kalnay, 2003).

The initialization of forecasts (and thus DA) plays a critical role in NWP as the more complete the information the analysis state has about the atmosphere, the longer pursuant forecasts will retain skill (e.g. Toth and Buizza, 2018). Hence the desire for DA to exploit as many observations, and from as diverse a set of instruments as possible. Some observations are in the form of model variables, in which case, after temporal and/or spatial interpolations, they can be directly combined with a model first guess (i.e., "direct" measurements or observations). Many other instruments, however, observe quantities that are different but ~~can be~~ related to the model variables (i.e., "indirect" measurements).

Indirect observations in the form of visible wavelength light intensity such as those from high (down to 30 second time frequency and 500m pixel) resolution imagers aboard a family of geostationary satellites (e.g., Himawari, GOES-R Advanced Baseline Imager, ABI, Schmit et al., 2017), and from airborne or ground-based cameras offer unique opportunities. First, unlike most other observations, light intensity is readily convertible to color imagery, offering a visual representation of the environment to both specialized (researchers or forecasters) and lay (the general public) users. Note that by far, visual perception is humans' most informative sense. Secondly, high resolution color imagery provides a unique window into fine-scale land surface, aerosol, and cloud processes that are critical both for the monitoring and nowcasting

of convective and other severe weather events, as well as for the assessment and refinement of modeled energy balance relationships crucial for climate forecasting. Information on related processes derivable from currently available other types of observations is limited in spatiotemporal and other aspects compared to color imagery.

Physically, color imagery is a visual representation of the intensity of different wavelength light (i.e. spectral radiance) reaching a selected point (i.e., location of a photographic or imaging instrument) from an array of directions determined by the design of the instrument, at a given time. For computational efficiency, radiative processes are vastly simplified in NWP models and typically resolve (Sun to atmospheric or land surface gridpoint) only how solar insolation, in a one dimensional manner, affects the temperature conditions in the atmosphere and on the land surface.

Color imagery clearly reflects (no pun intended) the geographical distribution and physical characteristics of cloud, aerosol, and land surface conditions in the natural environment. Some of the ~~related~~ quantities used in NWP models to represent such conditions include the amount of moisture, various forms of cloud forming and falling hydrometeors, the amount and type of aerosols, as well as the amount and type of vegetation and snow cover on the ground, and water surface wave characteristics ~~on the ground~~. Light processes recorded in color imagery constitute indirect measurements of such natural process that before their possible use in the initialization of NWP models, must be quantitatively connected with NWP model prognostic variables.

In the assimilation of direct observations, the value of model variables in the first guess is adjusted toward that of observations (based on the expected level of error in each, (~~e~~e.g. Kalnay, 2003). In the first step of assimilating indirect observations, simple models (called "forward" models or operators) are used to create "synthetic" observations based on model variables. Synthetic observations simulate what measurements we would get had instruments been placed in a world consistent with the abstract ~~world~~conditions of an NWP first guess forecast. The model-based synthetic observations then can be compared with real-world measurements of the same (non-model) quantities. Utilizing an adjoint, or ensemble-based inverse of the forward operator, or other minimization procedure, the first guess forecast variables are then adjusted to minimize the difference between the simulated and real observations. In case of visible light measurements, observations can be considered to be in the form of color (or multi-spectral visible) imagery.

~~It is important to point out that beyond~~Beyond their expanding use in DA applications, the simulation of color imagery from model variables via forward operators has another important purpose~~. This is~~: the visualization of 4D NWP analysis and forecast fields ~~(3 dimensions in space and one across model variables), making such complex data, as pointed out above, readily absorbable by both expert and lay audiences. ¶~~
~~¶~~
. Visualization renders the complex NWP data laid out in 3 dimensions in space and one across model variables) readily perceptable by both expert and lay audiences, facilitating a unique validation and communication of analysis and forecast information.

This study is intended to introduce SWIm, and describe what has been done so far, and suggest a roadmap for the future. Section 2 is a brief review of the general properties and limitations of currently available multispectral radiance and color imagery forward operators. The main contribution of this paper is the introduction of the recently developed fast color imagery forward (or color visible radiation transfer) model called Simulated Weather Imagery (SWIm, Section 3). Section 4 explores two application areas for SWIm: the visualization and validation of NWP analysis and forecast fields, as well as a vision for the assimilation of color imagery observations into NWP analysis fields. Closing remarks and some discussion are offered in Section 5.

2. Color Imagery and Spectral Radiance Forward Modeling

Light observations used in ~~color~~multispectral visible imagery are affected by three main factors: (1) the light source (its location and intensity across the visible spectrum); (2) the medium through which the light travels (the composition and density of its constituents in 3D space); and (3) the location where the light is observed or perceived (Fig. ~~3.~~1). Conceptually, the modeling of how light from a given source ~~would propagate~~propagates through a medium and ~~affect~~affects an instrument or receptor involves a realistic (a) relative placement of the light source, medium, and receptor with respect to each other ~~(prescribed)~~; (b) representation of light emission from its source ~~(prescribed)~~; (c) description of the medium (from an NWP analysis of the atmosphere and its surroundings); (d) simulation of how light is modified as it travels through the medium via absorptive and diffusive processes; and (e) simulation of the response of the instrument or human observer to the natural stimuli. Full, end-to-end color imagery forward modeling involves the specification of (a) and (b), ~~and based on the conditions of the medium estimated in~~an estimation of

(c), the simulation of processes described in (d) ("ray-tracing"), as well as the consideration of the impact of radiation (e).

Light propagation has been extensively studied from both experimental and theoretical perspectives. The scientifically most rigorous treatment involves the study of how individual photons are affected by, and a stochastic analysis of, the expected or net effect of scattering and absorption. Named after the stochastic concept involved, this line of inquiry and the related methodology is called the "Monte Carlo" approach. As ~~seen from figure 2.1, the~~noted in Table 1, a Monte Carlo approach (e.g., Mayer, 2009) works in a wide variety of situations with ~~the~~a wide array of 3-D atmospheric fields, arbitrary vantage points, and day/night applications. ~~Figure 2.1~~The Monte Carlo is the only listed package the authors have seen that produces similar images with visually realistic colors as seen from the ground. Table 1 also lists the characteristics of some other widely used radiative transfer models. Whereas the Monte Carlo (MC) model is physically more rigorous, it is computationally much more intensive than some of the other methods. The computational efficiency of the other methods come at a cost of significant approximations or other limitations. For example, the Rapid Radiative Transfer Model (RRTM) provides irradiance at different grid levels and is used as a radiation parameterization package in NWP models. As typical for such packages, RRTM operates in single columns, hence it cannot produce 3-D directional imagery that the Monte Carlo approach can. The Community Radiative Transfer Model (CRTM, Kleespies et al., 2004) is used for both visualization and as a radiative forward operator in variational and related DA systems. The Spherical Discrete Harmonic Ordinate Method (SHDOM, Evans, 1998, Doicu et al., 2013) is another sophisticated radiative transfer model often used in fine scale research studies. SHDOM can produce imagery with good physical accuracy.

~~Figure 2.1~~Table 1 also lists the characteristics of SWIm, the recently developed method that the next section describes in some detail. SWIm was designed for the rapid production of color imagery under a wide range of conditions. To satisfy ~~such a requirement~~these requirements, approximations to the more rigorous treatment of some physical processes had to be made. The level of approximations was carefully chosen to improve computational efficiency without unnecessarily sacrificing accuracy. By considering human color vision perception, SWIm ~~can also produce~~produces images that are visually realistic. This ~~is a unique feature that~~feature is used in other visualizations (e.g. Klinger et al, 2017) that use MYSTIC (Mayer, 2009), though to our knowledge isn't always considered for image display in the operational meteorology community. The color calculation allows the simulated images to be directly compared with photographic color images since it can accurately convert spectral radiance values

into appropriate displayed RGB values on a computer monitor as described in Section 3.8. As discussed in the rest of this study, with these features, SWIm occupies a niche for the versatile visualization and validation of NWP analyses and forecasts, as well as ~~in~~for the assimilation of color imagery observations aimed at ~~the improved initialization of NWP forecasts~~improved NWP initialization and nowcasting applications.

3. Ray Tracing Methodology

SWIm considers the ~~sun in the daytime and the moon at night~~Sun and the Moon (if it is sufficiently bright) as nearly point day- and night-time light sources. Information on the medium through which light travels is obtained from 3-D NWP analysis and forecast hydrometeor and aerosol fields. To simulate the propagation of light, SWIm invokes an efficient simplified ray tracing approach that can be benchmarked against results from more sophisticated radiative transfer packages, including the Monte Carlo method. There are two main ~~stages of ray tracing~~sets of rays that are traced for scattering and absorption calculations. The first is from the sun (forward direction, step 1a in Table 2) and the second is from the observer (backward direction, step 1b), making SWIm a forward-backward ray-tracing procedure (see FIg. ~~3.1~~1). These traces are ~~done on~~calculated over the model grid for the gas, aerosol, and hydrometeor components. Since the actual atmosphere extends above and if it is a limited area model (LAM), also laterally outside the model grid, an additional separate and faster ray-tracing step is done that considers just the gas and horizontally uniform aerosol components beyond the limited model domain. An algorithmic procedure then combines these results to arrive at the final radiance values and corresponding image display. The above steps are summarized in Table ~~1~~2 below.

¶

~~Step 1a: Forward rays from sun (in 3-D grid, including hydrometeors)¶~~
~~Step 1b: Backward rays from observer (in 3-D grid, including hydrometeors)¶~~
~~Step 2: Rays from sun and from observer (in clear air, extending beyond model grid)¶ ¶~~
~~Step 3: Combination of radiance components, generate RGB image display.¶~~

~~Table 1. List of ray tracing steps used in SWIm. Steps 1a and 1b are illustrated in Fig. 3.1.¶~~

For gas and aerosols, we evaluate the optical depth, τ, to determine transmittance T, where $T = \frac{I}{Io} = e^{-\tau}$. τ is the number of mean free paths. Io is the initial

intensity of the light beam and I is the attenuated intensity. The extinction coefficient β is integrated along the beam path to yield the optical depth. Thus¶
¶
:

$$\frac{d\tau}{ds} \tau = \int \beta \, ds = \alpha$$

(1)
¶
where ds is a distance increment traveling along the light ray. and¶

$$\tau = \int \alpha \, ds \quad (2)$$

The initial forward ray-tracing (step 1a) from the sun through the 3-D grid is tantamount to applying a radiative transfer algorithm to produce a 3-D short wave radiation field. This step is shown as the yellow rays in Fig. 3.1. We obtain 3-D hydrometeor and aerosol fields from either the analysis (00-hour forecast), or forecast (after the 00-hour initialization)(Step 1a, shown as the yellow rays in Fig. 1) is tantamount for producing a 3-D short wave radiation field. For visually realistic color imagery generation, ray-tracing is done multi-spectrally in three wavelength bandsat three reference wavelengths λ corresponding to the primary colors of human vision and display devices: 615nm (Red), 546nm (Green) and 450nm (Blue). The calculated radiances are represented in the software using an internal variable that is scaled to the solar spectral radiance at the top of the atmosphere. The light source is the sun in the daytime with the moon being used at night if it is sufficiently brightspecific wavelengths were chosen as a compromise between the locations of peaks in the Commission Internationale de l'Eclairage (CIE) color matching functions (Section 3.8) and a desire to have more uniformly spaced wavelengths that give independent samples of the visual (and solar) spectrum. The calculated radiances are scaled to the solar spectral radiance at the top of the atmosphere.

3.1 Solar irradiance and radiance

The top of atmosphere (TOA) solar irradiance E E_{TOA} at normal incidence is given by(sun located at zenith) is assumed to be $\frac{1362\ W/m^2}{r^2}$ where r is the Sun-Earth distance in astronomical units. This TOA irradiance can be expressed in terms of spectral irradiance E_λ $E_{TOA,\lambda}$ by considering the solar spectrum in units of W/m^2/nm. We can consider the SWIm image output in the form of spectral radiance L_λ in the spherical image space. L_λ corresponds to surface brightness and customarily is represented in

units of W/m^2/sr/nm. For numerical convenience the spectral radiance can be normalized to be in solar relative units based on the TOA solar spectral irradiance, distributed (e.g. scattered) in a hypothetical uniform fashion over the spherical image space ~~having an extent~~extending over a solid angle of 4π steradians. We will denote solar normalized (or relative) spectral radiance using the symbol L'_λ. Thus

¶

~~$L_\lambda = L'_\lambda \frac{E_\lambda}{4\pi}$~~ $L'_\lambda = \frac{4\pi L_\lambda}{E_{TOA,\lambda}}$ ~~(3)~~¶

¶

~~and~~¶

¶

~~.~~ (2)

It is interesting to note that sunlight reflected from a white Lambertian surface oriented normal to the sun has ~~$L'_\lambda = \frac{4\pi L_\lambda}{E_\lambda}$~~ $L'_\lambda = 4$ ~~(4)~~.

Once we calculate SWIm ~~image~~spectral radiance values at each pixel it is possible to estimate the Global Horizontal Irradiance (GHI) by ~~integrating the image radiance values over the hemispherical sky dome. The GHI is a wide spectrum measurement typically made from about 300nm to 3000nm. SWIm considers~~first integrating spectral radiance weighted by $cos(z)$ over the solid angle of the hemispherical sky to yield spectral irradiance. The GHI is typically calculated by integrating the spectral radiance from 300nm to 3000nm. However, SWIm only samples wavelengths within a narrower range from 400nm to 800nm. Despite this inconsistency, we can ~~take advantage of the fact that~~make an assumption when integrating over the ~~wide spectrum,~~wider spectrum that the resulting ~~radiance~~irradiance is nearly proportional to the spectral ~~radiance at 540nm. The proportionality holds for the solar spectrum, and typical modifications of this spectrum resulting from Rayleigh and Mie scattering. For example a normalized Rayleigh spectrum has more intensity in the blue wavelengths and less in the red and IR compared with the solar spectrum. The break even point is close to 540nm, and happens to be close to the 550nm standard often used to represent the peak sensitivity in human vision. This is borne out in preliminary case studies~~irradiance at the 546nm green wavelength used in SWIm calculations. This approximation is reasonably accurate in cases where the global irradiance has a similar spectrum to the incident solar radiation, as seen on a mostly cloud-free day in Fig. 2. For example the slight reddening of the direct solar radiation due to Rayleigh scattering is often partially compensated by the blue color of the sky that represents the diffuse irradiance. Overcast sky conditions should work as well as long as the sky is a relatively neutral

gray color. Indeed, the existing algorithm generally provides a close match when comparing SWIm generated GHI values to actual GHI values measured with a pyranometer at the National Renewable Energy Laboratory (NREL), in Golden, CO. We are presently working to refine this algorithm with a correction parameter based on atmospheric water vapor content, since this does have a more selective effect in the near-IR wavelengths. Similar calculations can be made for direct and diffuse solar irradiance. ¶

¶

3.2 Moonlight, city lights, and other light sources¶

¶

During the night the moon can replace the sun as an angularly localized light source (e.g., Miller et al., 2009). In the present study, the lunar radiance is calculated from considerations of its astronomical magnitude as a function of phase angle (180° – scattering angle). Near full moon a correction is added based on the opposition effect and potential lunar eclipses. At phase angles of less than ~4° the brightness is increased by up to ~20%, except the brightness is reduced substantially to factor in lunar eclipses as we move closer to 0° phase angle. Near new moon a term for Earthshine is taken into account, since this becomes significant compared with reflected sunlight from the lunar crescent. Earthshine is sunlight reflected first from the Earth's surface, then from the moon's surface. ¶

¶

Other light sources such as city lights, airglow, zodiacal light, individual stars and galactic glow are also included. An approximate scattering calculation is performed for city lights emanating from spatially extended areas with respect to the gas, aerosols, and cloud components of the atmosphere.¶

¶

Since the Earth can be approximated as a spherical object, various twilight phenomena can be displayed via spherical geometry accommodated by SWIm. The varying path of light through the curved atmosphere enables the reproduction of observable optical effects, including changes in clear sky and cloud colors. Effects relating to the Earth's shadow (including blockage by the terrain and attenuation by the lower atmosphere) are also represented, affecting both the molecular atmosphere and cloud related radiative processes. The "Belt of Venus" can be simulated when a moderate amount of high-altitude aerosols scatter red light just above the Earth's shadow, except it tends to overestimate the GHI in uniform overcast conditions. We are considering whether this is due to the radiative transfer assumptions in SWIm or an underestimation in the analyzed 3D hydrometeors and associated cloud optical thickness.

In a worst case scenario of a pure Rayleigh blue sky, we calculate that the normalized spectrum integrated from 0.3 μ to 3.0 μ has a crossover point at 530nm with the solar spectrum, yielding an irradiance underestimation of about 11% of the diffuse component when a SWIm reference green wavelength of 546nm is used. With a high sun in a clear sky this reduces to about 1% total GHI error since the Rayleigh scattered diffuse component is a small proportion of the total irradiance. For this error estimation, we integrated the Planck function at 5800K to represent an approximate solar spectrum and compared this with the Planck function convolved with the λ^{-4} intensity vs wavelength associated with Rayleigh scattering. The error be reduced by a more detailed consideration of the three SWIm reference wavelengths. A simple preliminary correction parameter based on atmospheric water vapor content has been added to account for absorption in the near-IR wavelengths. This presently neglects separate consideration of direct and diffuse solar irradiance.

3.2 Other light sources and atmospheric effects

With its realistic 3D ray tracing, SWIm is able to simulate a number of daytime, twilight, and nighttime atmospheric light effects, including consideration of a spherical atmosphere. This involves various light sources including moonlight, city lights, airglow, and astronomical objects. These will be demonstrated in a separate paper.

3.3 Clear sky ray-tracing

To cover the full extent of atmosphere beyond the NWP model domain, a “clear sky” ray-tracing (Step 2) is conducted ~~though~~ on a coarser angular grid compared with Step 1. The primary purpose of Step 2 is to provide a more direct account of the radiance produced by Rayleigh single scattering. A second purpose is to model the effect of aerosols that may extend beyond the top of the model grid, specified via a 1-D stratospheric variable. ~~Both~~The accuracy of radiative processes associated both with stratospheric aerosols and twilight ~~phenomena~~ benefit from the vertical extent considered in this step, all the way up to about 100km. To calculate the solar relative spectral radiance, the ray-tracing algorithm integrates along each line of sight from the observer as

$$L'_{\lambda,clear} = P(\theta) \int e^{-\tau_s} e^{-\tau_o} d\tau_o \qquad (3)$$

where θ is the scattering angle shown in Fig. 1 and $P(\theta)$ is the phase function (described in section 3.4.1). τ_s is the optical thickness along the forward ray (yellow

lines in Fig. 1) between the light source and each point of scattering and τ_o is the optical thickness along the backward ray (purple lines in Fig. 1) between the observer and each scattering point. We will denote this to be the clear sky radiance, that includes the molecular component through the full atmospheric depth and aerosols above the model grid top.

3.4 Hydrometeors

As the light rays are traced through the model grid (yellow rays in Fig ~~3.1.) their attenuation~~. 1, Step 1a in Table 2) their attenuation and forward scattering is determined by considering the optical thickness of intervening clouds and aerosols along their paths. ~~A two-stream approach is used to incorporate the backscatter fraction~~The optical thickness between each 3D grid point and the light source τ_s is calculated. An estimate of back-scatter fraction b is incorporated to help determine the ~~total downward illumination~~scalar irradiance E_λ (direct + ~~forward~~ scattered) at a particular model grid point. b is assigned a value of $.063$ for cloud liquid and rain, $.14$ for cloud ice and snow, and $.125$ for aerosols. Scalar irradiance is the total energy per unit area impinging on a small spherical detector. Based on a cloud radiative transfer parameterization (Stephens, 1978), a simplified version was developed for each 3D grid point as follows,

$$T_1 = 1 - \frac{b\tau_s}{(1+b\tau_s)} \qquad (4)$$

where T_1 is the transmittance of a cloud assuming light rays are scattered primarily along a straight line from light source to grid point. We define auxiliary eq. 5 that assumes some light rays can have multiple scattering events that travel predominantly perpendicular to an assumed horizontal cloud layer and z_0 is the solar zenith angle. This allows for cases with a vertical cloud thickness significantly less than horizontal extent, and the multiply scattered light will largely travel in an envelope that curves on its way from the light source to the observer.

$$T_2 = 1 - \frac{b\tau_s \cos z_0}{(1 + b\,\tau_s \cos z_0)} \qquad (5)$$

Eq. 6 is used on the assumption that the overall transmittance T will depend on the dominant mode of multiple scattering between source and observer, either along a straight line T_1, or the light scatters mostly perpendicular to the cloud layer T_2, allowing a shorter path to travel through the hydrometeors.

$$T = max(T_1, T_2 \cos z_0) \quad (6)$$

Considering the direct ~~illumination~~irradiance component, the hydrometeor extinction coefficient is largely dependent on the effective radius of the cloud hydrometeor size distribution. The expression in eq. ~~5~~7 is adapted from (Stephens, 1978).

~~$\alpha = \frac{1.5\,CWC}{r_e \varrho_h}$~~ $\beta = \frac{1.5\,CWC}{r_e \varrho_h}$

(~~5~~ (7)

~~Where~~ β is the extinction coefficient used when we integrate along the light ray from the light source the grid point to calculate τ_s, CWC is the condensed water content, r_e is the effective radius, and ϱ_h is the hydrometeor density based on the hydrometeor type and the effective radius -- all defined at the current model grid point.

The effective radius is specified based on hydrometeor type and (for cloud liquid and ice) CWC. For cloud liquid and cloud ice, larger values of CWC translate to having larger r_e and smaller β. In other words larger hydrometeors have a smaller area to volume ratio and scatter less light per unit mass. When we trace light rays through a particular grid box, the values of CWC are ~~bilinearly~~trilinearly interpolated to help prevent rectangular prism shaped artifacts from appearing in the images.

We can now write eq. 8 for the scalar irradiance at the grid point, here assuming the surface albedo to be 0,

$$E_{x,y,z,\lambda} = e^{-\tau_R}\, T\, E_{TOA,\lambda} \quad (8)$$

where τ_R represents the optical thickness of the air molecules between the light source and observer that engage in Rayleigh scattering. Light reflected from the surface or scattered by air molecules and reaching the grid point are neglected here and considered in subsequent processing.

3.4.1 Single Scattering

The single scattering phase function has a sharp peak near the sun (i.e. forward scatter) that generally becomes stronger in magnitude for larger hydrometeors. Cloud ice and snow also have sharper forward peaks than liquid, particularly for pristine ice. A linear combination of Henyey-Greenstein (HG) functions (Henyey and Greenstein, 1941) is employed to specify the angularly dependent scattering behavior (phase function) for

each hydrometeor type, producing curves shown in Figure 3.23. Linear combinations employing several of these functions are used as a simple way to reasonably fit the angular dependence produced by Mie scattering. If more detailed size distributions (and particle shapes for ice) are available, a more exact representation of Mie scattering can be considered through the use of Legendre polynomial coefficients and a lookup table, or through other parameterizations (e.g. Key et al., 2002). Given the values of asymmetry factor g, the individual Henyey-Greenstein terms (6) are formulated herecombined and normalized to integrate to a value of 4π over the sphere, so that their average (normalized) value is 1, thus conserving energy. θ is the scattering angle (Fig. 1), and i represents an individual HG phase function term that is linearly combined to yield the overall phase function. Specific values of f_i and g_i are given in expressions for $P_{thin}(\theta,\lambda)$ in section 3.4.2 and in Appendix B. These provide for light scattered in both forward and backward directions.

$$P_i(\theta) = p_i(\theta, g_i) = \frac{1 - g_i^2}{[1 + g_i^2 - 2g_i\, cos(\theta)]^{3/2}}$$

(69)

The overall phase function is given by

¶

$$P(\theta) = \sum_i c_i P_i(\theta) \quad P(\theta) = \sum_i f_i\, p_i(\theta, g_i)$$

(7)¶

, (10)

noting that $\sum_i f_i = 1$. When $\tau << 1$ $\tau_o << 1$ we can use a thin atmosphere approximation to estimate the solar relative spectral radiance due to single scattering.

$$L_\lambda' \simeq P(\theta)\,\tau \quad L_\lambda' \simeq P(\theta)\,\tau_o\omega$$

(8 . (11)

This relationship applies to hydrometeors as well as aerosols and the molecular atmosphere. In practice, the ray tracing algorithm considers extinction between the sun and the scattering surface as well as between the scattering surface and the observer., thus eq. 11 applies given also that $\tau_s << 1$ along the ray traced from the observer. ω is the single scattering albedo as discussed below in Section 3.5.1. To allow a more general handling of larger values of τ_s a more complete formulation of the solar relative radiance is as follows:

$$L_{\lambda}^{'} = P(\theta) \int_{\tau_o=0}^{2} E\, e^{-\tau_o}\, d\tau_o \quad . \quad (12)$$

3.4.2 Multiple scattering

When the optical thickness along the forward or backward paths approaches or exceeds unity, contributions to the observed signal from multiple scattering events become too significant to approximate via single-~~scatter~~scattering. A rigorous, though time-consuming approach such as Monte-Carlo would consider each scattering event explicitly. Instead, here we use a more efficient approximation that arrives at a single scattering phase function that approximates the bulk effect of the multiple scattering events. Several terms that interpolate between optically thin and thick clouds are used as input for this parameterization as described below.

Thick clouds seen from near ground level can be either directly or indirectly illuminated by the light source. ~~Inspection of~~As illustrated by the light rays in ~~figure 3.1 helps show that~~Figure 1, direct ~~-~~illumination corresponds to $lim_{\tau_o \to 0}\ \tau_s = 0$. A fully lit cloud surface will by definition have no intervening material between it and the sun. Conversely, indirect illumination implies that $lim_{\tau_o \to 0}\ \tau_s >> 0$. The indirect illumination case is assumed to have anisotropic brightness that is dependent on the upward viewing zenith angle z of each image pixel. This modulates the transmitted irradiance value associated with the point where this light ray intersects the cloud. ~~For an example with a heavy overcast sky, we use~~ Note that when looking near the horizon, the multiple scattering events have a higher probability of having at least one surface reflection, resulting in an increased probability of photon absorption. Under conditions of heavily overcast sky and low surface albedo, this results in a pattern of a darker sky near the horizon and a steadily brightening sky toward the zenith. Such a pattern typically seen in corresponding camera images is reasonably reproduced with the use of a normalized brightness given by $\frac{1 + 4\cos(z)}{3}$ ~~, providing a darker sky near the horizon and a steadily brightening sky toward the zenith. This generally matches observed camera images in cases with low surface albedo. A rationale for this is that when looking near the horizon, the multiple scattering events have a higher probability of having at least one surface reflection, resulting in an increased probability of photon absorption.~~. The direct illumination case is similar except that the irradiance value is given by the solar irradiance and the relative brightness depends on the scattering angle, peaking in the antisolar direction.

Intermediate values of τ_o are given empirical phase functions with decreasing effective values of g as τ_o increases, similar to the concepts described in Piskozub and McKee, 2011. As τ_o increases with thicker clouds, the scattering order also increases and the effective phase function becomes flatter. When $\tau_o > 1$, we consider an effective asymmetry parameter $g' = g^{\tau_o}$, where g is the asymmetry parameter term used for single scattering. The strategy of using g' in the manner shown below underscores the convenience of using HG functions in the single scattering phase function formulation. g' is combined with additional empirical functions that help give simulated cloud images that are similar to observed clouds of varying optical thicknesses. The goal is to have the solar aureole gradually expanding with progressively thicker clouds, eventually becoming diluted into a more uniform cloud appearance. In the case of cloud liquid, looking at a relatively dark cloud base where $\tau_s >> 1$, we arrive at this semi-empirical formulation for the effective phase function.

$$P(\theta,\lambda,z) = c_1 P_{thin}(\theta,\lambda) + c_2 P_{thick}(\theta,z) \ , \tag{13}$$

where c_1 and c_2 are weighting coefficients.

$$c_1 = e^{-(\tau_o/10)^2} \frac{E_\lambda}{E_{TOA,\lambda}} \quad \text{and} \tag{14}$$

$$c_2 = 1 - c_1 \ . \tag{15}$$

Given the empirical nature of this formulation, $c_1 + c_2$ isn't constrained to equal 1. For optically thin clouds we calculate P_{thin} considering the three reference wavelengths λ introduced in section 3 and associated asymmetry parameters g_λ:

$$g_\lambda = (0.945,\ 0.950,\ 0.955) \tag{16}$$

$$f_1 = 0.8 \times \tau_o \tag{17}$$

$$P_{thin}(\theta,\lambda) = f_1\, p(\theta, g_\lambda^{\tau_o}) + (1.06 - f_1)\, p(\theta, 0.6^{\tau_o}) + 0.02\, p(\theta, -0.6) - 0.08\, p(\theta, 0) \tag{18}$$

$P_{thick,h}$ represents the effective phase function of a directly illuminated (high radiance) optically thick cloud, typically the sunlit side of a cumulus cloud. We represent such clouds as sections of spherical surfaces with a surface brightness varying as a function of θ.

Our neighboring planet Venus offers an astronomical example for the radiative behavior of such a cloudy spherical surface. For the planet as a whole, Venus has a well established phase function $\triangle m$ (in astronomical magnitudes, Mallama et al., 2006). Changes in the average radiance of the illuminated portion of the sphere can be approximated by dividing the total brightness (numerator of eq. 19) by the illuminated fractional area. This denominator is based on its current illuminated phase (or equivalently the scattering angle θ).

$$P_{thick,h}(\theta) = \frac{(1.94 / 10^{(0.4 \times \triangle m(\theta))})}{(1 - cos(\theta)) / 2} \tag{19}$$

The effective phase function of an indirectly illuminated thick low irradiance cloud (e.g., a dark cloud base, $P_{thick,l}$) can be written as:

$$P_{thick,l}(z) = \frac{1 + 2\,cos(z)}{3} \tag{20}$$

We combine the high irradiance and low irradiance cases for thick clouds depending on the irradiance of the surface of the cloud facing the observer, such that

$$P_{thick}(\theta, z) = 2\,c_3\,P_{thick,h}(\theta) + 4\,c_4\,P_{thick,l}(z)\,. \tag{21}$$

c_3 and c_4 are further weighting coefficients blending the component phase functions such that

$$c_3 = e^{-(\tau_o/10)^2}\,\frac{E_\lambda}{E_{TOA,\lambda}} \quad \text{and} \tag{22}$$

$$c_4 = 1 - c_3\,. \tag{23}$$

The coefficients were experimentally determined by comparing simulated images of the solar aureole from clouds having various thicknesses, with both camera images and visual observations. Similarly constructed effective phase functions are utilized for cloud ice, rain, and snow (Appendix B).

3.4.3 Cloud Layers Seen from Above

As a simple illustration for cases looking from above we consider a homogeneous cloud of hydrometeors having optical thickness τ, being illuminated with the sun at the zenith

(i.e. $z_o = 0$). The cloud albedo (assuming a dark land surface) can be parameterized as:

$$a = \frac{b\tau}{(1+b\tau)} \quad \text{(9}$$

. (24)

where b is the backscatter fraction (Stephens, 1978). τ here is considered to be along the slant path of the light rays coming from the sun (τ_s in Fig. 3.11). For values of $\tau \leq 1$, we can assume single scattering and $a \sim b\tau$, while for large τ, $a > 0.9$ and asymptotes to just below 1.0 (not reaching 1.0 identically due to the presence of a very small absorption component term). We set b based on a weighted average of the contribution to τ along the line of sight for the set hydrometeor types. Cloud liquid and rain use $b = .06$, cloud ice and snow use $b = .14$. Graupel has yet to be tested in SWIm, though we anticipate using $b = .30$.

For $\tau >> 1$ (asymptotic limit) the cloud albedo a can be translated into an approximate reflectance value through a division by μ_o, where $\mu_o = cos\, z_o$. This is the case since thick cloud (or aerosol) layers act approximately as Lambertian reflectors (with $g \to 0$) for the high order scattering component (Piskozub and McKee, 2011, Gao et al., 2013, Bouthers et al., 2008). When a given photon is scattered many times, the stochastic nature of the scattering causes the correlation between the direction of propagation of the photon and the direction of incident radiation to greatly decrease. To improve the accuracy so we canwe address the anisotropies that do occur when looking at cloud layers from above. A simple bidirectional reflectance distribution function (BRDF) is thus being developed in the form of an anisotropic reflectance factor (ARFoccur using a bidirectional reflectance distribution function (BRDF) as specified with a simple formula for the anisotropic reflectance factor (ARF).

$$ARF = \frac{b_1 + b_2\, cos(z)\, cos(z_0) + P(\theta, g, f_b)}{4\, cos(z)\, cos(z_0)} \quad (25)$$

z is the zenith angle of the observer as seen from the cloud. A DHG phase function (eq. 27) is used as a simple approximation for an assumed water cloud where $g = 0.7$ and $f_b = 0.4$. This parameterization (Kokhanovsky, 2004) using $b_1 = 1.48$ and $b_2 = 7.76$ produces results consistent with graphical plots depicting the ARF for selected solar zenith angles (Lubin and Weber, 1994). When all orders of scattering are considered, the ARF remains relatively close to 1 when the solar zenith anglezenith angles z_o, z_o isare small. A large solar zenith angle will showshows preferential forward scattering causing the ARF to increase markedly with low scattering angles. Even with this

enhancement, inspection of ABI satellite imagery suggests the reflectance factor, $\mu_o \times ARF$, generally stays below 1.0 in forward scattering cases.

In cases where ~~$\tau < 1$~~ $\tau < 1$ we are in a single scattering (or low-order) regime and the dependence of reflectance on μ_o goes away. In practice, this means that thicker aerosol (or cloud) layers will generally decrease in reflectance with a large z_o, while the reflectance holds more constant for very thin layers (assuming molecular scattering by the gas component is small). This causes the relative brightness of thin aerosol layers, compared with thicker clouds and the land surface to increase near the terminator. ~~Interpolation is used to approximate the reflectance between~~Linear interpolation with respect to cloud albedo is used to arrive at an expression for solar relative radiance taking into account the low τ and high τ regimes.¶

¶

~~**3.5 Aerosols**~~¶

¶

~~SWIm applications in a Multidisciplinary University Research¶~~
~~Initiative (MURI) called "Holistic Analysis of Aerosols in Littoral Environments" (HAALE) required improvements to the treatment of atmospheric aerosol.~~

$$L_\lambda^{'} = P(\theta)\,(1-a) + ARF\ a \qquad (26)$$

Here $P(\theta)$ is specified in Eq. 13. It should be noted that absorption within thick clouds has yet to be included in specifying the cloud albedo.

3.5 Aerosols

There are two general methods for working with aerosols in SWIm. The first uses a 1-D specification of the aerosol field that runs somewhat faster than a 3-D treatment. The second, newer, approach considers the 3-D aerosol distribution described in detail herein. Aerosols are specified by a chemistry model in the form of a 3-D extinction coefficient field. Various optical properties are assigned based on the predominant type (species) of aerosols present in the model domain.

3.5.1 Single Scattering

To determine the scattering phase function clouds and aerosols are considered together and aerosols are simply considered as another species of hydrometeors. For a case of aerosols only, the phase function $P(\theta)$ is defined depending on the type of aerosol. The

Double Henyey-Greenstein (DHG, eq. 27) function (Louedec et al., 2012) is the basis of what is used to fit the phase function.

$$P(\theta, g, f_b) = (1 - g^2)\left[\frac{1}{1+g^2-2g\cos(\theta)} + f_b\left(\frac{3\cos^2(\theta)-1}{2(1+g^2)^{3/2}}\right)\right] \quad (10\ (27)$$

This function has the property of integrating to 1 over the sphere representing all possible light ray directions - θ is the scattering angle, and the asymmetry factor g represents the strength of the forward scattering lobe. The weaker lobe in the back scattering direction is controlled by f_b.

Dust generally has a bimodal size distribution of relatively large particles. ~~For this~~Accounting for both the coarse and fine mode aerosols, and for fitting the forward scattering peak, a linear combination of a pair of DHGs (eq. 11) can be set by substituting g_1 and g_2 for g. As an example we can assign $g_1 = .962$, $g_2 = .50$, $f_b = .55$, $f_c = .06$, where f_b is the term for the backscatter peak and f_c is the fraction of photons assigned to the first DHG using g_1:

$$P(\theta, g_1, g_2, f_b) = f_c P(\theta, g_1, f_b) + (1 - f_c) P(\theta, g_2, f_b) \quad (\text{~~11~~}28)$$

Smoke and haze are composed of finer particles. Here we can also specify a combination of g_1, g_2, and f_c to help in fitting the phase function. The asymmetry factor values of g, g_1 and g_2 each have a slight spectral variation to account for the variation in size parameter with wavelength. This means that a slight concentration of bluer light occurs closer to the sun or moon. The overall asymmetry factor g is related to the component factors g_1 and g_2 as follows:

$$\text{~~}g = f_c g_1 + (1 - f_c) g_2\text{~~}\ g = f_c g_1 + (1 - f_c) g_2 \quad (\text{~~12~~}29)$$

g_1 and g_2 are allowed to vary slightly between the three reference wavelengths (Section 3). In addition, each application of the DHG function uses an extinction coefficient that varies according to an Angstrom exponent, that in turn depends on ~~the asymmetry factor g~~ g at 546nm. This allows for the spectral dependence of extinction. Coarser aerosols will have a higher asymmetry factor (i.e. a stronger forward scattering lobe), a lower Angstrom exponent and a more uniform extinction at various wavelengths

giving a more neutral color. The value of f_c can be set to reflect contributions from a mixture of aerosol species. We can thus specify the aerosol phase function with four parameters g_1 , g_2 , f_c , and f_b .

The single scattering albedo ω can also be specified for each wavelength to specify the fraction of attenuated light that gets scattered. ω represents the probability that a photon hitting an aerosol particle is scattered rather than absorbed, thus darker aerosols have ω significantly less than 1. The spectral dependence of ω is most readily apparent in the color of the aerosols as seen with back scattering. This applies either to a surface view opposite the sun, or to a view from above (e.g. space). Taking the example of hematite dust, the single scattering albedo ω is set to 0.935, 0.92, and 0.86 for our Red/Green/Blue reference wavelengths, respectively. This can eventually interface with a library of optical properties for a variety of aerosol types.

3.5.2 ~~Aerosol~~ Optical Properties Assignment

In its current configuration, aerosol optical properties for the entire domain are assumed to be characterized by a single set of parameters in SWIm, reflecting the behavior of a predominant type or mixture of aerosols. The first row in Table ~~2 was derived~~3 was arrived at semi-empirically for relatively dusty days in Boulder, CO ~~based on a comparison between simulated and camera images and visual observations.~~ , by setting values of the parameters and comparing the appearance of the solar aureole and overall pattern of sky radiance between simulated and camera images as well as visual observations.

The cameras being used aren't radiometrically calibrated, though we can approximately adjust the camera color and contrast on the basis of the Rayleigh scattering radiance distribution far from the sun on relatively clear days. We are thus limited to looking principally at relative brightness changes in a semi-empirical manner. The cameras aren't using shadow bands, and generally have saturation due to direct sunlight within ~5-10 degrees radius from the sun. In some cases we supplement the cameras with visual observations (e.g. standing behind the shadow of a building) to assess the innermost portions of the aureole.

These days feature a relatively condensed aureole around the sun indicative of a contribution by large dust particles to a bimodal aerosol size distribution. This type of distribution has often been observed in AERONET (Holben et al., 1998) retrievals. The single scattering albedo is set with increased blue absorption as might be expected for dust containing a hematite component.

The second case of mixed dust and pollution was derived from AERONET observations over Saudi Arabia, calculating the phase function using Mie scattering theory (Appendix A), then applying a curve fitting procedure to yield the four phase function parameters described previously. In this case the single scattering albedo is spectrally independent. Simulated images for these two sets of phase function parameters are shown in Fig. 3.34.

¶

Case¶	g_1 ¶	g_2 ¶	f_c ¶	f_b ¶	ω ¶
Colorado Dust¶	.59, .60, .61¶	.895, .900, .905¶	.12, .12, .12¶	.550, .550, .550¶	.935, .92, .86¶
Saudi Arabian Mixed Dust and Pollution¶	.23, .27, .29¶	.915, .925, .933¶	.58, .54, .53¶	.562, .558, .558¶	.96, .96, .96¶

¶

Table 2. Two cases showing the four fitted phase function parameters g_1 , g_2 , f_c , and f_b as well as single scattering albedo ω , for each of the three reference wavelengths, 615nm, 546nm and 450nm. ¶

¶

3.5.3 Aerosol3.5.3 Multiple Scattering

As with meteorological clouds, when the aerosol optical thickness along the forward or backward ray paths (Fig 3.11) approaches or exceeds unity, the contributions from multiple scattering increase. As with cloud multiple scattering, a rigorous approach such as Monte-Carlo would consider each scattering event explicitly, though this would be computationally inefficient. Once againIn a manner similar to cloud multiple scattering, we appeal toutilize a more efficient approximation that determines a single scattering phase function that is equivalent to the net effect of the multiple scattering events.

3.5.4 Aerosol Layers Seen from Above

Non-absorbing aerosols seen from above can be treated in a similar manner to cloud layers as described above (eq. 69). We now extend this treatment to address absorbing aerosols. Along with 3-D aerosol fields from the CIRA chemistry (RAMS and WRF) model analyses and forecasts,SWIm was tested using 3D aerosol fields from two

chemistry models running at Colorado State University (CSU): the Regional Atmospheric Modeling System (RAMS, Miller et al., 2019; Bukowski et al., 2019) and the Weather Research and Forecasting Model (WRF, Skamarock et al., 2008). SWIm was also tested with two ~~other~~additional chemistry models, ~~HRRR~~the High Resolution Rapid Refresh (HRRR)-Smoke (Fig ~~3.5~~5, available at https://rapidrefresh.noaa.gov/hrrr/HRRRsmoke) and the Navy Global Environmental Model (NAVGEM - Fig ~~3.4). This~~6, Hogan et al., 2014). These tests yielded valuable information about how multiple scattering in absorbing aerosol layers can be handled.

For partially absorbing aerosols such as smoke containing black carbon or dust, in a thin layer we can multiply eq. (6) by ω, the single scattering albedo to get the aerosol layer albedo.

$$a = \omega \frac{b\tau}{(1+b\tau)} \qquad (\text{~~13~~}30)$$

A more challenging case to parameterize is when $\tau \gg 1$ and multiple scattering is occurring. Each extinction event where a photon encounters an aerosol particle now also has a non-zero probability of absorption occurring. Here we can consider a probability distribution for the number of scattering events for each photon that would have been received by the observer if the aerosols were non-absorbing (e.g. sea salt where $\omega \sim 1$). We can define a new quantity ω' to represent a multiple scattering albedo.

$$a = \omega' \frac{b\tau}{(1+b\tau)} \qquad (\text{~~14~~}31)$$

For typical smoke or dust conditions a will approach an asymptotic value between about 0.3 to 0.5. We plan to check the consistency of SWIm assumptions with previous work in this area such as in (Bartkey, 1968). Once the albedo is determined a phase function is used for thin aerosol scattering and a BRDF is used for thick aerosols. This is similar to the way that clouds are handled.

3.6 Combined clear sky and aerosol/cloud radiances

The clear sky radiance $L'_{\lambda,clear}$ is calculated through the whole atmosphere in Step 2, while the aerosol and cloud radiances (grouped into $L'_{\lambda,cloud}$) are determined within the more restricted volume of the model grid (Step 1b). As a post-processing step these

quantities are merged together with this empirical procedure to provide the combined radiance $L_\lambda^{'}$ at each location in the scene from the observer's vantage point.¶
We define a quantity f_{front} to be the conditional probability that a backward traced light ray from the observer is scattered or absorbed by the molecular component vs. being scattered or absorbed from the molecular component, aerosols, or hydrometeors. τ_1 is denoted as the optical thickness of the molecular and aerosol component between the observer and where $\tau_o = 1$ (τ_o also having hydrometeors included). We then calculate the following:

$$f_{clear} = f_{front} + (1 - f_{front})\,(1 - e^{-\tau_o}) \quad (32)$$

$$f_{cloud} = (1 - e^{-\tau_o})\, e^{-\tau_1} \quad (33)$$

$$L_\lambda^{'} = f_{clear}\, L_{\lambda,clear}^{'} + f_{cloud}\, L_{\lambda,cloud}^{'} \quad (34)$$

The above strategy permits the addition of blue sky from Rayleigh scattering in front of a cloud, based on the limited amount of atmosphere between observer and cloud.

3.7 Land Surface

When a backward-traced ray starting at the observer intersects the land surface we consider the incident and reflected light upon the surface that contributes to the observed light intensity, as attenuated by the intervening gas, aerosol, and cloud elements. Terrain elevation data on the NWP model grid is used to help determine where light rays may intersect the terrain. The land spectral albedo is obtained at 500m resolution using the Blue Marble Next Generation Imagery (BMNG, Stockli et al., 2005). The BMNG image RGB values are functionally related to spectral albedo for three Moderate Resolution Imaging Spectroradiometer (MODIS) visible wavelength channels. A spectral interpolation is performed to translate the BMNG / MODIS albedos into the three reference wavelengths used in SWIm.

For higher resolution display over the continental United States, an aerial photography dataset obtained from the United States Department of Agriculture (USDA) can also be used (Figs ~~3.6, 3.7~~7, 8). The associated National Agriculture Imagery Program (NAIP) data are available at 70cm resolution and is added to the visualization at sub-grid scales with respect to the model Cartesian grid. This dataset is only roughly controlled for spectral albedo, though it can be a good tradeoff with its very high spatial resolution.

To obtain the reflected surface radiance in each of the three reference wavelengths, we utilize clear-sky estimates of direct and diffuse incident solar irradiance. For the direct irradiance component, spectral albedo is converted to reflectance using the anisotropic reflectance factor ~~f~~ ARF that depends on the viewing geometry and land surface type. Thus ~~the~~ reflectance ~~$\varrho = af$~~ ϱ is defined as: $\varrho = a\,(ARF)$, where a is the terrain albedo. ~~We calculate the~~The solar relative spectral radiance of the land surface is calculated as

$$L_\lambda' = \frac{4\,\varrho\,E_{\lambda H}}{E_\lambda} \qquad (\text{~~15~~}35)$$

where $E_{\lambda H}$ is the global horizontal spectral irradiance. This relationship can also be used for the diffuse irradiance component if we assign ~~$f = 1.$~~ $ARF = 1.$

Relatively simple analytical functions for ~~f~~ ARF are used over land with maximum values in the backscattering direction. Modified values of surface albedo and ~~f~~ ARF are used in the presence of snow or ice cover with maximum values in the forward scattering direction. A sun glint model with a fixed value of mean wave slope is used over water similar to earlier work (Cox and Munk, 1954), except that waves are given a random orientation without a preferred direction. Scattering from below the water surface is also considered. In the future, wave slope will be derived from NWP ocean wave and wind forecasts.

~~Terrain elevation data on the NWP model grid is used to help determine where light rays may intersect the terrain. ¶~~

3.8 Translation into displayable color image

As explained earlier, spectral radiances are computed ~~within the software~~ for three narrowband wavelengths, using solar-relative intensity units to yield a scaled spectral reflectance. This allows some flexibility for outputting spectral radiances, spectral reflectance, or more visually realistic imagery that accounts for details in human color vision and computer monitor characteristics. To accomplish the latter it is necessary to estimate spectral radiance over the full visible spectrum using the partial information from the selected narrowband wavelengths we have so far. Having a full spectrum is important when computing an accurate human color vision response (Bell et al., 2006). The procedure is to first perform a polynomial interpolation and extrapolation of the three narrowband (solar relative) reflectance values, then multiply this by the solar

spectrum, ~~helping to fill the gaps and yield full spectral radiance information~~yielding spectral radiance over the entire visible spectrum at each pixel location. The observed solar spectrum interpolated in 20nm steps is used for purposes of subsequent numerical integration. ~~Having a full spectrum is important when computing an accurate human color vision response [Bell et al., 2006].~~

Digital RGB color images are created by calculating the image count values with three additional steps:

1) Convolve the spectral radiance (produced by the step described in the above paragraph) with the CIE tristimulus color matching response functions to account for color perception under assumptions of normal human photopic vision. Each pixel of the image now specifies the perceived color in the XYZ color space (Smith and Gould, 1931). In this color system the chromaticity (related to color hue and saturation) is represented by normalized xy values and the perceived brightness is the Y value. The normalization of the XYZ values to yield chromaticity specifies that x+y+z=1. The xyz chromaticity values represent the normalized perception for each of the three primary colors. An example illustrating the benefits of this procedure is the blue appearance of the daytime sky. We calculate a pure Rayleigh blue sky to have chromaticity values of x=.235, y=235. The violet component of the light is actually stronger than blue, but has less impact on the perceived color since we are less sensitive to light at that wavelength.

2) Apply ~~the~~a 3x3 transfer matrix that puts the XYZ image into the RGB color space of the display monitor.

$$\begin{bmatrix} r \\ g \\ b \end{bmatrix} = \begin{bmatrix} 3.1894 & -1.5755 & -.4948 \\ -.9735 & 1.8951 & 0.0376 \\ 0.0635 & -.2160 & 1.2244 \end{bmatrix} \begin{bmatrix} X \\ Y \\ Z \end{bmatrix} \quad (36)$$

This is needed in part because the colors of the display system are not spectrally pure. Another consideration is the example of spectrally pure violet light, perceived in a manner similar to purple (a mix of blue and red for those with typical trichromatic color vision). Violet is beyond the wavelengths that the blue phosphors in a monitor can show, so a small component of red light is mixed in to yield the same perception, analogous to what our eye-brain combination ~~will do~~does. We make the assumption that the sun (the main source of illumination) is a pure white color as is very nearly the case when seen from space thus setting the white point to ~~5800K~~5780K, the

sun's approximate color temperature. Correspondingly, when viewing SWIm simulated color images, we also recommend setting one's display (e.g. computer monitor) color temperature to ~~5800K.~~ 5780K.

3) Include a gamma (approximate power law) correction with a value of 2.2 to match the non-linear monitor brightness scaling. ~~This is important if we want~~With this correction the displayed image brightness ~~to~~will be directly proportional to the actual brightness of ~~the~~a scene in nature, giving realistic contrast and avoiding unrealistically saturated colors. ¶

¶

~~This procedure is anticipated to give~~With no correction, the contrast would be incorrect and the brightness off by an exponential amount.

Based on an extensive subjective assessment, this procedure gives a realistic color and contrast match if one looks at a laptop computer monitor held next to ~~the scene (with either ground~~a scene in a natural setting on the ground, and is anticipated to perform well for air- ~~or~~and space-based ~~viewing)~~simulations as well. The results have somewhat more subtle colors and contrast compared with many commonly seen Earth and sky images ~~that we see~~. The intent here is to make the brightness of the displayed image proportional to the actual scene, and the perceived color to be the same as a human observer would see in a natural setting. This is without any exaggeration of color saturation ~~prevalent~~sometimes occurring in satellite "natural color" image rendering (e.g. Miller et al., 2012) and even in everyday photography (subjective observation, Albers 2019). For example color saturation values of the sky in photography often exceeds the calculated values for even low aerosol conditions. A more complete consideration of the effects of atmospheric scattering and absorption in SWIm image rendering softens the appearance of the underlying landscape when viewed from space or otherwise afar. This is due to SWIm not suppressing the contribution of Rayleigh scattering to radiance as observed in nature.

4. Applications¶

¶

~~4.1 Demonstration~~ of SWIm ~~–~~

4.1 Model Visualization

~~As we've seen, a~~The fast 3-D radiative transfer package called Simulated Weather Imagery ~~(SWIm)~~ has been developed to serve ~~in several roles relating to high-resolution model development and implementation. For example, visually~~the development and

application needs of high-resolution atmospheric modeling. Visually and physically realistic ~~images in~~, full natural color (e.g., Miller et al., 2012) ~~help to display output from model~~ SWIm imagery, for example, offers a holistic display of numerical model output (analyses and forecasts). At a glance one can see critical weather elements such as the fields of clouds, precipitation, aerosols and land surface in a realistic and intuitive manner. Model results are thus more effectively communicated for interpretation, displaying weather phenomena that ~~can be seen~~we see in the sky and ~~surrounding environment. SWIm readily conveys~~contront in the surrounding environment. NWP information about current and forecast weather is readily conveyed in an easily perceivable visual form to both scientific and lay audiences.

The SWIm package has ~~been~~ run ~~an~~on a variety of NWP modeling systems including the ~~LAPS Weather Research and Forecasting (WRF) system, Colorado State University (CSU) Regional Atmospheric Modeling System (RAMS) model, HRRR~~Local Analysis and Prediction System (LAPS, Toth et al., 2014), WRF, RAMS, HRRR (Benjamin et al., 2016), and NAVGEM. We can thus discern general characteristics of the ~~models~~respecting data assimilation and modeling systems including their handling of clouds, aerosols, and land surface (e.g. snow cover).

4.1.1 CSU RAMS Middle East Dust Case

Visualization of the RAMS model developed at ~~Colorado State University~~CSU was done for a case featuring dust storms over the Arabian Peninsula and the neighboring region (Miller et al., 2019; Bukowski et al., 2019), as part of the Holistic Analysis of Aerosols in Littoral Environments Multidisciplinary University Research Initiative (HAALE-MURI) ~~project~~. Figure ~~4.1~~9 shows the result of this simulation from in-situ vantage points just offshore from Qatar in the Persian Gulf at altitudes of 4km and 20m above sea level. With the higher vantage point we are above most of the atmospheric dust present in this case, so the sky looks bluer with ~~Rayleigh scattering being more dominant~~the Rayleigh instead of Mie scattering being more dominant.

4.1.2 ~~Additional~~Other Modeling Systems

Figure ~~3.5~~5 shows a space-based perspective of the December 2017 wildfires in Southern California using NWP data from the HRRR-Smoke system. Smoke plumes from fires and areas of inland snow cover are readily visible. SWIm has been most thoroughly tested with another NWP system called the Local Analysis and Prediction System (LAPS, Albers et al., 1996, Jiang et al., 2015). LAPS produces very rapid (5-minute) update and very high resolution (e.g. 500-m) analyses and forecasts of 3-D

fields of cloud and hydrometeor variables. The LAPS cloud analysis is a largely sequential data insertion procedure that ingests satellite (including IR and 500-m resolution visible imagery, updated every 5-min), ground-based cloud cover and height reports, radar, and aircraft observations along with a first guess forecast. This scheme is being updated with a 3/4DVAR cloud analysis module that in the future will also be used in other fine scale data assimilation systems.

Figure ~~3.6~~7 depicts a simulated panoramic view from the perspective of an airplane cockpit at 1km altitude using LAPS analysis with 500m horizontal resolution. This is part of an animation designed to show how SWIm can be used in a flight simulator for aviation purposes. ~~The visualization is using~~This visualization uses sub-grid scale terrain albedo derived from USDA 70cm resolution airborne photography acquired at a different time. SWIm has also been used to display LAPS-initialized WRF forecasts of severe convection (Jiang et al., 2015) showing a case with a tornadic supercell that produced a strong tornado striking Moore, Oklahoma in 2013.

4.2 Validation of NWP analyses and forecasts

~~Simulated images and animations can be used by data assimilation and model developers as a validation to assess model performance and help guide improvements in initial and forecast fields, respectively. The imagery provides a qualitative validation of both the model fields and the visualization package when simulated images are compared against actual camera images. If in various situations simulated imagery can well reproduce observed images, this is an indication of the realism of the radiative transfer / visualization package (i.e., SWIm). Discrepancies between simulated and observed images in other cases may be interpreted as shortcomings in the analyzed or model forecast states. ¶~~

~~¶~~

~~The vantage point for such assessments can be~~ from a variety of vantage points (on the ground, in the air, or ~~from~~in space~~, (~~i.e. with multi-spectral visible satellite data)~~. At a glance various obstructions to visibility can be intuitively seen in the imagery such as clouds, haze, and smoke. The land surface state including snow cover, visibility and illumination can be assessed. Figure 4.3 shows a cloud-free sky comparison where aerosol loading was relatively high due to smoke. ¶~~

~~¶~~

~~Solar irradiance computed by a solid angle integration of SWIm imagery can be compared with corresponding pyranometer measurements. For space-based satellite imagery, color images can be compared qualitatively and visible band reflectance can be used for quantitative comparison.¶~~

¶

~~SWIm has been tested with a variety of models. An example is an NWP system that produces very rapid update (5-15min) and very high resolution (e.g. 500m) analyses and forecasts (Local Analysis and Prediction System - LAPS, Toth et al., 2014). The cloud analysis (Albers et al., 1996, Jiang et al., 2015) of LAPS uses satellite (including IR and 1-km resolution visible imagery, updated every 15-min), METAR, radar, and aircraft observations along with a first guess forecast to produce 3-D fields of cloud and hydrometeor variables. The LAPS cloud analysis is running regionally at 500m horizontal resolution on a 5- to 10-min update cycle. The 3-D hydrometeor fields are analyzed using satellite, radar, surface ceilometer observations, and model first guess fields. The largely sequential data insertion procedure of today's LAPS is being updated with a 3/4DVAR cloud analysis module that in the future will be used both in LAPS and other fine-scale data assimilation systems.~~ can be used by developers to assess and improve the performance of numerical model and data assimilation techniques. A subjective comparison of simulated imagery against actual camera images serves as a qualitative validation of both the model fields and the visualization package itself. If simulated imagery can well reproduce observed images under a representative range of weather and environmental conditions, this is an indication of the realism of the radiative transfer / visualization package (i.e., SWIm). Discrepancies between simulated and observed images in other cases may be due to shortcomings in the analyzed or model forecast states.

Comparing analyses from LAPS with day-time and night-time camera images under cloudy, precipitating, and clear/polluted air conditions, SWIm was tested and can realistically reproduce ~~rainbows, twilight sky colors and other~~various atmospheric phenomena (Albers and Toth, 2018). Since camera images are not yet used as observational input in LAPS, subjective and quantitative comparisons of high resolution observed and simulated weather imagery provides a valuable opportunity to assess the quality of cloud analyses and forecasts from various NWP systems, including LAPS, Gridded Statistical Interpolation (GSI~~)~~, ~~High Resolution Rapid Refresh (HRRR)~~Kleist et al., 2009), HRRR, Finite Flow Following Icosahedral Model (FIM, Bleck et al, 2015), and the NAVGEM.

360° imagery, presented in either a polar or cylindrical projection, can show either analysis or forecast fields. Here, we present the results of ongoing developments of this simulated imagery, along with comparisons to actual camera images produced by a network of all-sky cameras that is located within our Colorado 500m resolution domain, as well as space-based imagery. These comparisons (summarized in Table 4) check the

skill of the existing analysis of clouds and other fields (e.g. precipitation, aerosols, and land surface) at high-resolution.

4.2.1 Ground-based observations

Figure 4.210 shows a comparison between a simulated all-sky image and an observed camera viewand a camera observed all-sky image valid at the same time. The simulated image was derived from a LAPS cloud analysis running at 500m horizontal resolution on a, 5-min update cycle. The camera image LAPS cloud analysis. Assuming realistic ray tracing and visualization, the comparison provides an independent validation of the analysis. In this case we see locations of features within a thin high cloud deck are reasonably well placed. Variations in simulated and observed cloud opacity (and optical thickness) are also reasonably well matched. This is evidenced by the intensity of the light scattering through the clouds relative to the surrounding blue sky, as well as the size (and shape) of the brighter aureole closely surrounding the sun. The brightness scaling being used for both images influences the apparent size of the the inner bright (saturated) part of the solar aureole in the imagery. This saturation can occur either from forward scattering of the light by clouds and aerosols or from lens flare. The size also varies with cloud optical thickness and reaches a maximum angular radius at $\tau \sim 3$.

It is also possible to compare simulated and camera images to validate gridded fields of model aerosol variables. In figure 4.3 we see such a comparison usingparticular, the effects of constituents other clouds, such as haze, smoke, or other dry aerosols on visibility under conditions analyzed or forecast by NWP systems can also be instantly seen in SWIm imagery (Albers and Toth 2018). Analogous to Fig. 10 (except its panoramic projection), Figure 11 shows a cloud-free sky comparison where aerosol loading was relatively high due to smoke. LAPS uses a simple 1-D aerosol analysis for a smoky day in Boulder, Colorado when the AOD was measured by a nearby AeronetAERONET station to be 0.7. ¶

¶

4.2.2 Space-based observations The area within $\sim 5^{\circ}$ of the sun in the camera image should here be ignored due to lens flare.

Alternatively, solar irradiance computed by a solid angle integration of SWIm imagery has been compared (initially via case studies) with corresponding pyranometer measurements (Fig. 10). Qualitative comparison of the land surface state including snow cover and illumination can be compared with camera observations (not shown).

4.2.2 Space-based observations

For space-based satellite imagery, color images can be compared qualitatively and visible band reflectance can be used for quantitative comparisons.

Figure ~~4.4~~12 shows observed imagery from the Earth Polychromatic Imaging Camera (EPIC) imagery aboard the Deep Space Climate Observatory (DSCOVR, Marshak et al, 2018) satellite, used as independent validation in a comparison with ~~a simulated image~~an image simulated by SWIm from a Global LAPS (G-LAPS) ~~fields visualized using SWIm. The analysis shown here comprises 3-D cloud liquid and cloud ice fields hourly~~analysis. The DSCOVR imagery was empirically reduced in contrast to represent the same linear brightness (image gamma - Sec. 3.8) relationships used in SWIm processing. The LAPS analysis comprises 3-D hydrometeor fields (four species) at 21km resolution, in addition to other state and surface variables such as snow and ice cover. Visible and IR satellite imagery are utilized from GOES-16 and GOES-17, with first guess fields from a ~~GFS forecast~~Global Forecast System (GFS) forecast, an operational model run by the National Oceanic and Atmospheric Administration (NOAA).

The horizontal location and relative brightness of the simulated vs. observed clouds match fairly closely in the comparison for many different cloud systems over the western hemisphere. The land surface spectral albedo also appears to be in good agreement, including areas of snow north of the Great Lakes. The sun glint model in SWIm shows the enhanced brightness surrounding the nominal specular reflection point in the ocean areas surrounding the Yucatan peninsula due to sunlight reflecting from waves assumed to have a normal slope distribution. This can help with evaluation of a coupled wind and ocean wave model. There is some difference in feature contrast due to a combination of cloud hydrometeor analysis (e.g. the brightest clouds in central North America) and SWIm reflectance calculation errors, as well as uncertainty in the brightness scaling of the DSCOVR imagery, along with uncertainties in the snow albedo used in SWIm over vegetated terrain. The ~~DSCOVR~~EPIC imagery ~~was empirically reduced in contrast to represent the same linear brightness (image gamma - Sec. 3.8) relationships used in SWIm processing.~~ shown was obtained from the displayed EPIC web products with color algorithms unknown to the authors, thus a better comparison could be performed using the radiance calibrated EPIC data, adjusted for Earth rotation offsets for the three color channels. The color image comparison is shown here to give an intuitive illustration of a multispectral comparison. The reflectance factor distribution for both SWIm and DSCOVR (now using the calibrated L1b radiance data)

in a single channel (the red band) matches anticipated values from 5% in darkest clear oceanic areas to ~1.1 in bright tropical convection.

Figure ~~4.5~~13 shows a comparison of ~~the RAMS model run discussed earlier with a corresponding color image generated from MODIS Aqua data. Features representing lofted dust are depicted over~~color images over the Arabian peninsula and over the Persian Gulf as generated from MODIS Aqua observations and via SWIm simulation from a RAMS model forecast. Various environmental conditions such as lofted dust (near the Arabian peninsula and over the Persian Gulf~~. Liquid~~), liquid (low) and ice (high) clouds can be seen. The microphysics and chemistry formulations in the RAMS model can be assessed and improved based on this comparison, such as minimizing an excess of cloud-ice in the model simulation. The amount of dust east of Qatar over the water appears to be underrepresented in this model ~~run~~forecast.

4.2.3 Objective measures

In advanced validation and data assimilation applications (Section 4.3) ~~applications~~ an objective measure is ~~desired~~needed for the comparison of observed and simulated imagery. For simple measures of similarity, cloud masks can be derived from both a SWIm and a corresponding camera image, using for example sky color (e.g. red/blue intensity ratios). Categorical skill scores can then be used to assess the similarity of the angular or horizontal location of the clouds.

To assess the spatial coherence of image values (thus radiances) between the simulated and observed images, the Pearson correlation coefficient r can be ~~used~~determined as

$$r = \frac{N\sum xy - \sum x \sum y}{\sqrt{[N\sum x^2 - (\sum x)^2][N\sum y^2 - (\sum y)^2]}} \quad , \qquad (37)$$

where N is the number of pixel pairs and x, y are the pixel pair values. The mean value of r, calculated individually for the set of simulated vs. observed pixel intensities in each of the image channels R, G, B, is denoted as $\bar{r}$. We consider this to be a measure of overall image similarity. The R channel is generally most sensitive to clouds and large aerosols, with blue emphasizing Rayleigh scattering contributions from air molecules and Mie scattering from small aerosols. The G channel is sensitive to land surface vegetation and sky colors that can occur around sunset and twilight. Over many cases

of SWIm vs. camera image comparisons, $\bar{r}$ was found to correspond well to the subjective assessment of the sky spectral radiance patterns, circumventing ~~biases~~potential bias arising due to a lack of radiance calibration in many types of cameras. ¶

¶

Note that $\bar{r}$ values ~~reveal~~are shown for image comparisons presented in Figs. 11 and 14.

in addition to feature characteristics and locations, $\bar{r}$ values are also affected by how realistic the optical and microphysical properties of the analyzed clouds and aerosols are~~, in addition to feature locations. When~~. In other words, when $\bar{r}$ < 1, this reflects possible deficiencies in the quality of (i) the 3D digital analysis or specification of hydrometeors, aerosols, and other variables; (ii) the calibration of observed camera images, and (iii) the realism or fidelity of the SWIm algorithms. Recognizing that (a) with all their details, visible imagery is high dimensional and good matches are extremely unlikely to occur by chance, and that (b) high $\bar{r}$ values attest to good performance in all three aspects listed above (i, ii, and iii), the occurrence of just a few cases with high $\bar{r}$, as long as they span various atmospheric, lighting, and observing position conditions, may be sufficient to demonstrate the realism of the SWIm algorithms. For example, the correlation coefficient between the two images in figure ~~4.3~~11 is 0.961, indicating the smoke induced aureole around the sun (caused by forward scattering) is well depicted by SWIm. ¶

¶

~~**4.3 Assimilation of camera and satellite imagery**~~To improve the accuracy of the $\bar{r}$ metric in future investigations we are instituting a 5° exclusion radius around the sun to mask out lens flare.

4.3 Assimilation of camera and satellite imagery

Today, NWP model forecasts predominate most weather prediction applications from the hourly to the seasonal time scales. Fine scale (up to 1 km) nowcasting in the 0-60 or -120 minutes time range is the notable exception. It cannot even be evaluated whether numerical models lack realism on such fine scales as relevant observations are sporadic and no reliable 3D analyses are available on those scales, which would also be needed for successful predictions. No wonder: NWP forecasts are subpar compared with statistical or subjective methods in hazardous weather warning applications. It is a catch 22 situation: model development is hard without a good analysis, and quality analysis is challenging to do without a good model - this is the latest frontier of NWP development. The comparisons presented in Figs. 10 and 12 offer a glimmer of hope

that model evaluation and initialization may one day be possible with advanced and computationally very efficient tools prototyped in a simple fashion with SWIm and LAPS as examples.

With new geostationary satellite instruments ~~such as~~(e.g. ABI) now available, ~~we have~~ an abundance of high-resolution satellite data ~~in the~~are available in spatial, temporal, and spectral domains. As ground-based camera networks also become more readily available we envision a unified assimilation of camera, satellite, ~~and other~~radar, and other, more traditional and new data sets in NWP models. SWIm can be used with camera images (and possibly visible satellite images) as a forward operator to constrain model fields in a variational minimization. One approach ~~would entail developing SWIM's~~entails the development and use of SWIm's Jacobian or adjoint, while other techniques employ recursive minimization. ~~Observed camera images can thus be assimilated within a 3/4DVAR cloud analysis module. 3D- and 4DVAR has been proposed to utilize infrared and visible satellite data (Vukicevic et al., 2004, Polkinghorne and Vukicevic, 2011). ¶~~

~~¶~~

Vukicevic et al., 2004 and Polkinghorne and Vukicevic, 2011 proposed to assimilate infrared and visible satellite data using 3D- and 4DVAR methods. Likewise, observed camera images can also be assimilated within a 3/4DVAR cloud analysis module. Such capabilities may be useful in NWP systems such as GSI, the Joint ~~Environment~~Effort for Data assimilation Integration (JEDI~~), variational LAPS (vLAPS), and various global models. Thus~~, https://www.jcsda.org/jcsda-project-jedi), vLAPS (Jiang et al., 2015), or other systems.

SWIm can be ~~combined~~used in conjunction with other forward operators (such as the CRTM and SHDOM~~) for comparison with camera and satellite data~~, to compare simulated with observational ground, air, or space based camera data in various wavelengths or applications. Along with additional ~~observational data~~types of observations (e.g., RADAR, METARs)~~,~~ and model physical, statistical, and dynamical constraints ~~we can provide~~(e.g., using the Jacobian or adjoint), a more complete 3-D and 4-D variational assimilation ~~to drive a very fine scale cloud-resolving model. This moves toward the goal of having the model be more consistent with full resolution radar and satellite data. ¶~~

~~¶~~

~~We are experimenting with methodologies to use camera images for calculating a penalty term in a variational cost function. A promising approach is to utilize~~scheme can be constructed to initialize very fine scale cloud-resolving models. Such initial conditions may be more consistent with full resolution radar and satellite data. Note that on the

coarser, synoptic and sub-synoptic scales, adjoint-based 4D variational data assimilation (DA) methods such as that developed at the European Center for Medium Range Forecasts (ECMWF) proved superior to alternative, ensemble-based DA formulations. The authors are not aware of any credible arguments for why this would not also be the case for cloud scale initialization.

A variational 3D tomographic analysis highlighting precipitating hydrometeors was performed with airborne passive microwave observations (Zhou et al., 2014).
In recent years several groups have experimented with extraction and use of cloud information from camera images.An example solving for a 3D cloud mask using a ground-based camera network as discussed in (Viekherman et al., 2014). This has been expanded using airborne camera image radiances to perform a 3D cloud liquid analysis (Levis, Schechner, Aides, 2015; Levis, Schechner et al., 2015) using a similar forward operator (SHDOM) in a variational solver using a recursive minimization. A corresponding aerosol Observation Simulation Experiment OSE analysis (Aides et al., 2013) was also performed with a ground-based camera network. A design for tomographic camera-based cloud analysis has more recently been developed (Mejia et. al, 2018).

As an initial non-variational test, the authors experimented with the use of the $\bar{r}$ metric described ~~above. Two non-variational assimilation methods that are preliminary alternatives to using the Jacobian or adjoint have so far been tested with SWIm. One test (a single case run at this point) involves determining a translation vector applied to the entire 3D satellite-constrained cloud field to best fit the camera simulated image, maximizing~~in Section 4.2.3 above. This involves clearing existing, or adding new clouds based on cloud masks derived from color ratios seen in the simulated and/or actual camera images. A single iteration of an algorithm to modify the 3D cloud fields with the mask information often yields improvement in $\bar{r}$. ~~The second test involves constructing cloud clearing and adding masks based on color ratios seen in the simulated and/or actual camera images. A single iteration of an algorithm to modify the 3D cloud fields with the mask information often yields improvement in~~ judging from a series of real-time case studies. The removal of clouds just above the reference point, and additions in South and NNW direction resulted in increase of $\bar{r}$ ~~judging from a series of real-time case studies.¶~~
~~¶~~
~~To move towards the goal of comparing absolute radiance values~~from 0.407 to 0.705 in the example of Fig. 14. This improvement is consistent with visual inspection of clouds between the camera image (b) and the modified simulated image (c) vs. the simulated image from an analysis without the use of the ground-based camera image (a).

Since SWIm operates in three dimensions and considers multiple scattering of visible light photons within clouds it can help perform a 3D tomographic cloud analysis. To move towards the goal of comparing observed and simulated absolute radiance values in a variational setting, two strategies are being considered. The first strategy would entail more precise calibration of camera exposure and contrast so images can be directly compared using a root mean square statistic. A second strategy entails using the simulated image to estimate Global Horizontal Irradiance (GHI, Section 3.1) and then comparing with a GHI measurement made with a pyranometer colocated with the camera. ~~The GHI estimation examines a calculated field of spectral radiance at 550nm, then extrapolates this to the wavelength integrated radiance at each angular location. Correction factors based on atmospheric pressure and water vapor can be added. As earlier noted, colors in the sky such as Rayleigh scattering happen to have crossover points in their normalized spectra with the solar spectrum that is close to the 550nm reference wavelength. This can be exploited when the radiance values are integrated over the hemisphere, normalizing by~~

5. Discussion and Conclusion

To make SWIm more generally applicable, its ray tracing algorithms have been extended to address simulations with various light sources, optical phenomena (e.g. rainbows), and twilight colors (to be reported in future publications). Current SWIm development is focused on aerosol optical properties and multiple scattering. Ongoing work also includes refinements to the single scattering albedo and the phase function for various types of aerosols, including dust and smoke. The parameterization being used to determine effective multiple scattering albedo ~~$cos(z)$~~ ω' ~~to yield the irradiance.¶~~

~~¶~~

~~Since SWIm operates in three dimensions and considers multiple scattering of visible light photons within clouds it can help perform what is described as a tomographic cloud analysis. An example of tomographic analysis highlighting precipitating hydrometeors was performed with airborne passive microwave observations (Zhou et al., 2014). Further examples include solving for a 3D cloud mask using a ground-based camera network as discussed in (Vickherman et al., 2014). This has been expanded using airborne camera image radiances to perform a 3D cloud liquid analysis (Levis, Schechner, Aides, 2015; Levis, Schechner et al., 2015) using a similar forward operator (SHDOM) in a variational solver using a recursive minimization. A corresponding aerosol Observation Simulation Experiment OSE analysis (Aides et al., 2013) was also~~

performed with a ground-based camera network. A design for tomographic camera-based cloud analysis has more recently been developed (Mejia et. al., 2018). ¶

¶

5. Conclusions and Discussion¶

¶

A visualization package that performs a fast 3-D radiative transfer in visible wavelengths called Simulated Weather Imagery (SWIm) has been presented. As summarized in Fig. 2.1, SWIm produces radiances in a wide variety of situations, even though other packages are more rigorous for particular situations they are designed for, at an increased computational cost. SWIm can be used to simulate color imagery of weather, including land surface conditions based on NWP analysis or forecast data in a visually realistic manner. SWIm images thus can be used to make complex and abstract NWP forecasts perceptually accessible, to subjectively and objectively assess the quality of NWP products, as well as to assimilate observed imagery via a comparison of such with simulated imagery produced by SWIm from first guess NWP forecasts.¶

¶

An example of how SWIm can help forecasters with model interpretation and communication of weather information to the public is the possible dissemination of time-lapse sky camera views for both recent and future weather (is being revised to improve reflectance values associated with thick dust and smoke seen from space-based vantage points. Concurrently the improved parameterization of absorption with multiple-scattering will determine how dark it becomes for ground-based observers when heavy smoke and/or thick dust is present. Under these conditions, spectral variations in ω' become amplified as τ increases, causing the sky to have more saturated colors as it darkens.

A fast 3-D radiative transfer model in visible wavelength with a corresponding visualization package called Simulated Weather Imagery (SWIm) has been presented. As summarized in Table 1, SWIm produces radiances in a wide variety of situations involving sky conditions, light sources, and vantage points. Even though other packages are more rigorous for particular situations they are designed for, that comes at a significantly higher computational cost. The visually realistic SWIm color imagery of weather and land surface conditions makes the complex and abstract 3D NWP analyses and forecasts from which it is simulated from perceptually accessible, facilitating both subjective and objective assessment of NWP products. Initial use of SWIm has emphasized its role as a realistic visualization tool. Ongoing development and evaluation will allow SWIm to be used in a more quantitative manner in an increasing variety of situations. To date the evaluation has focused mainly on comparisons with ground-based cameras, pyranometers, and DSCOVR imagery, even

though they typically include the LAPS cloud analysis used for SWIm input in the evaluation pipeline. Specific comparisons with other radiative transfer packages (e.g. CRTM, MYSTIC) is a good topic for future work.

Validation of SWIm is summarized in Table 4 and consists of both qualitative and quantitative assessment. The quality of the hydrometeor and aerosol analysis plays a role, making these joint comparisons of SWIm and the analysis techniques. Additional quantitative validation is planned to compare SWIm with other 1D and 3D radiative transfer models in a manner that is more independent of analysis quality.

Simulated time-lapse sky camera views for both recent and future weather can be used, for example, for the interpretation and communication of weather information to the public (an archive of near real-time ~~and archived~~ examples available at http://stevealbers.net/allsky/allsky.html)~~.~~ Interactive 3D flythroughs ~~viewing~~viewed from both inside and above the model domain can be ~~an~~another exciting way to display NWP model results for both scientific and lay audiences. This includes the use of in flight simulators for aviation purposes, along with other interactive game engines. ¶
~~¶~~
~~Beyond the use of existing camera networks, the installation and use of >~~High quality images or animations from existing or to be installed all-sky cameras with greater than 180° field of view ~~all-sky cameras~~ at official meteorological or other observation sites could also be ~~considered. High quality animations constructed with images from such cameras could be~~ used to evaluate clouds, aerosols, and land surface features such as snow cover analyzed ~~and forecast by~~or forecast in NWP systems.~~-~~

~~The full~~A critical use of camera images in the future will ~~include~~be their variational assimilation into high-resolution analysis states for the initialization of NWP forecasts used in Warn-On-Forecasting (Stensrud et al., 2013). ~~This~~The comparison of high quality ground-, air-, or space-based camera imagery with their simulated counterparts is a critical first step in the assimilation of such observations. The assimilation of such gap-filling observations can be especially useful in pre-convective environments where cumulus clouds are present while radar echoes have yet to develop. Today's DA techniques suffer in such situations, severely limiting the predictability of tornadoes and other high impact events. 4-D variational tomographic DA is designed to combine camera and satellite imagery from multiple viewpoints. The sensitive dependence of multiple scattering in 3D visible wavelength light propagation on the type and distribution of hydrometeors facilitates a better initialization of cloud properties throughout the depth of the clouds. This in turn can potentially extend the time span of predictability for severe weather events from the current period starting with the

emergence of organized radar echoes back to the more subtle beginnings of cloud formation.

~~¶~~

~~Methods and results related to the use of various light sources and the simulation of various twilight phenomena will be covered in separate publications. Current development of SWIm is focused on aerosol optical properties and multiple scattering. Ongoing work includes refinements to the single scattering albedo and the phase function for various types of aerosols, including dust and smoke. The parameterization being used to determine ω' is being revised to improve reflectance values associated with thick dust and smoke seen from space-based vantage points. Concurrently the improved parameterization of absorption with multiple scattering will determine how dark it becomes for ground-based observers when heavy smoke and/or thick dust is present. Spectral variations in ω' become amplified as τ increases, causing the sky to have more saturated colors as it darkens.¶~~

As the spatiotemporal and spectral resolution of color imagery observed both with ground-based cameras or air- and satellite-borne instruments and corresponding output from NWP models reaches unprecedented highs, a question arises whether variational or other DA methods can sensibly combine information from the two sources? ~~Consistent~~If they can, consistent analyses of clouds and related precipitation and aerosol fields ~~would~~will aid situational awareness and fine-scale model initialization. SWIm used as a 3-D forward operator for camera and visible satellite imagery may help addressing the above and related ~~questions~~challenges.

Acknowledgements:

This work was ~~largely funded within the HALLE-MURI project supported by the Office of Naval Research (ONR~~partially funded by a Multidisciplinary University Research Initiative (MURI) called Holistic Analysis of Aerosols in Littoral Environments (HAALE). For the HAALE-MURI project the support of the Office of Naval Research under grant N00014-16-1-2040 is gratefully acknowledged. Additional funding was provided by NOAA under the Cooperative Institute for Research in the Atmosphere (CIRA). We thank Didier Tanre and the AERONET team for establishing and maintaining Capo Verde AERONET site used in this investigation. We also thank Afshin Andreas and Mark Kutchenreider of the National Renewable Energy Laboratory (NREL) in Golden Colorado, along with Will Beuttell of EKO Instruments Inc. for help in accessing their real-time all-sky camera images. We appreciate the helpful feedback and suggestions provided by two anonymous reviewers.

References:

Aides A., Schechner Y. et al., Multi sky-view 3D aerosol distribution recovery. Optics express 21 (22): 25820-33, doi: https://doi.org/10.1364/oe.21.025820, 2013.

Albers S., and Toth, Z., Visualization, Evaluation, and Improvement of NWP-Based Cloud Analyses and Forecasts, JCSDA Newsletter Quarterly, 61, 17-26, doi: 10.25923/jw00-r987, 2018.

Albers S. et al.: The Local Analysis and Prediction System (LAPS): Analyses of Clouds, Precipitation, and Temperature, Weather and Forecasting, 11, 273-287, 1996.

Bannister R., Elementary 4D-VAR, DARC Technical Report No. 2. Data Assimilation Research Centre, University of Reading, UK, 2007.

Bartkey, The Reflectance of Homogeneous, Plane-parallel Clouds of Dust and Smoke, J. Quant. Spectrosc. Radiat. Transfer. 8, 51-68, 1968.

Bell, J. F. III, D. Savransky D., and Wolff M.J., Chromaticity of the Martian sky as observed by the Mars Exploration Rover Pancam instruments, J. Geophys. Res., 111, E12S05, doi:10.1029/2006JE002687, 2006.

Benjamin et al.: A North American Hourly Assimilation and Model Forecast Cycle: The Rapid Refresh.Mon. Wea. Rev., 144, 1669-1694, doi: 10.1175/MWR-D-15-0242.1, 2016.

Bleck, R. et al.: A vertically flow-following icosahedral grid model for medium-range and seasonal prediction. Part I: Model description, Mon. Wea. Rev., 143, 2386–2403, doi:10.1175/MWR-D-14-00300.1, 2015

Bodhaine, B A et al.: On Rayleigh Optical Depth Calculations. JTech 16, 11, 1854-1861, 1999.

Bouthers et al.: Interactive multiple anisotropic scattering in clouds, Proceedings of the 2008 symposium on interactive 3D graphics and games, 173-182, doi: 10.1145/1342250.1342277, 2008.

Bukowski, J. and van den Heever, S. C.: Effect of horizontal model resolution on the convective redistribution of mineral dust over the Arabian Peninsula. Submitted to Appl. Chem. Phys., 2019.

Cox, C. and Munk, W.: Measurement of the Roughness of the Sea Surface from Photographs of the Sun's Glitter. J. Opt. Soc. Am. 44, 838-850, 1954.

Doicu, A., Efremenko D., and Trautmann, T.: A multi-dimensional vector spherical harmonics discrete ordinate method for atmospheric radiative transfer. J. Quant. Spectrosc. Radiat. Transfer, 118, 121-131, doi: https://doi.org/10.1016/j.jqsrt.2012.12.009 , 2013.

Dubovik, O., Sinyuk, A., Lapyonok, T., Holben, B. N., Mishchenko, M., Yang, P., Eck, T. F., Volten, H., Muñoz, O., Veihelmann, B., van der Zande, W. J., Leon, J.-F., Sorokin, M., and Slutsker, I.: Application of ~~spheriod~~spheroid models to account for aerosol particle nonsphericity in remote sensing of desert dust, J. Geophys. Res., 111, D11208, doi:10.1029/2005JD006619, 2006.

Evans, K. F.: The spherical harmonic discrete ordinate method for three-dimensional atmospheric radiative transfer. J. Atmos. Sci., 55, 429-446, 1998.
Henyey L.G. and Greenstein J.L.: Diffuse radiation in the galaxy, Astrophysical Journal 93:70-83, 1941

Gao M., Huang X., Yang P., and Kattawar G.W.: Angular distribution of diffuse reflectance from incoherent multiple scattering in turbid media, Appl. Opt. 52, 5869-5879, doi: https://doi.org/10.1364/AO.52.005869, 2013

Giles, D.M., Holben, B. N., Eck, T. F., Sinyuk A., Smirnov, A., Slusker I., Dickerson, R. R., Thompson, A. M., and Schafer, J. S.: An analysis of AERONET aerosol absorption properties and classifications representative of aerosol source regions, J. Geophys. Res., 117, D17203, doi:10.1029/2012JD018127, 2012.

Hogan F. et al.: The Navy Global Environmental Model, Oceanography, 27, 116-125. doi:10.5670/oceanog.2014.73, 2014

Holben, B.N., Eck,T.F., Slutsker, I., Tanre, D., Buis, J. P., Setzer, A., E.Vermote, E, Reagan, J.A., Kaufman, Y.,.Nakajima, T., Lavenu, F., Jankowiak, I., and A.Smirnov, A.: AERONET - A federated instrument network and data archive for aerosol characterization, Rem. Sens. Environ., 66, 1-16, 1998

Jiang H. et al.: Real-Time Applications of the Variational Version of the Local Analysis and Prediction System (vLAPS). Bulletin of the American Meteorological Society 96 (12), 2045-2057, doi: https://doi.org/10.1175/bams-d-13-00185.1, 2015.

¶

Kalnay E.: Atmospheric modeling, data assimilation and predictability. Cambridge university press, 341 pp., 2003.

Key, J., Yang, P., Baum, B., Nasiri, S.L.: Parameterization of shortwave ice cloud optical properties for various particle habits, JGR Atmospheres, 107, AAC 7-1-AAC 7-10, doi: 10.1029/2001JD000742, 2002.

Kleespies, T.J., van Delst P., McMillin L.M., and Derber, J., Atmospheric transmittance of an absorbing gas. 6. An OPTRAN status report and introduction to the NESDIS/NCEP Community Radiative Transfer Model, Appl. Opt., 43, 3103 – 3109, doi:10.1364/AO.43.003103, 2004.

Kleist, D.T., et al.: Introduction of the GSI into the NCEP Global Data Assimilation System. Weather and Forecasting, 24, 1691-1705, doi:10.1175/2009WAF2222201.1, 2009.

Klinger, C., et al.: Effects of 3-D thermal radiation on the development of a shallow cumulus cloud field. Atmospheric Chemistry and Physics, 17, 5477--5500, doi: 10.5194/acp-17-5477-2017, 2017.

Kokhanovsky, A.: Optical properties of terrestrial clouds. Earth-Science Reviews. 64. 189-241. doi:10.1016/S0012-8252(03)00042-4, 2004.

Levis A., Y. Schechner, Y., and Aides, A.: Airborne Three-Dimensional Cloud Tomography. 2015 IEEE International Conference on Computer Vision (ICCV) (2015): 3379-3387, doi: https://doi.org/10.1109/iccv.2015.386, 2015.

Levis A., Schechner Y., et al.: An Efficient Approach for Optical Radiative Transfer Tomography using the Spherical Harmonics Discrete Ordinates Method, arXiv:1501.06093, 2015.

Louedec, K., Pierre Auger Collaboration & Losno, R. Atmospheric aerosols at the Pierre Auger Observatory and environmental implications, Eur. Phys. J. Plus, 127: 97, 2012.

Lubin D., and Weber, P.: The use of Cloud Reflectance Functions with Satellite Data for Surface Radiation Budget Estimation, Journal of Applied Meteorology, 34, 1333-1347, 1995.

Mallama, T., Wang, D., Howard, R.: Venus phase function and forward scattering from H_2SO_4, Icarus 182(1), 10-22, doi: 10.1016/j.icarus.2005.12.014, 2006

Marshak, A., J. Herman, S. Adam, B. Karin, S. Carn, A. Cede, I. Geogdzhayev, D. Huang, L. Huang, Y. Knyazikhin, M. Kowalewski, N. Krotkov, A. Lyapustin, R. McPeters, K.G. Meyer, O. Torres, and Yang Y.: Earth Observations from DSCOVR EPIC Instrument. Bull. Amer. Meteor. Soc., 99, 1829–1850, doi:10.1175/BAMS-D-17-0223.1, 2018.

Mayer B.: Radiative transfer in the cloudy atmosphere. European Physical Journal Conferences., 1:75-99, 2009.

Mejia, F. A., Kurtz, B., Levis, A., de la Parra, I., and Kleissl, J.: Cloud tomography applied to sky images: A virtual testbed. Solar Energy. 176. 287-300, doi: 10.1016/j.solener.2018.10.023., 2018.

Miller, S. D., Grasso, L., Bian, Q., Kreidenweis, S., Dostalek, J., Solbrig, J., Bukowski, J., van den Heever, S. C., Wang, Y., Xu, X., Wang, J. Walker, A., Zupanski, M., Wu, T.-C., Chiu, C., and Reid, J.: A Tale of Two Dust Storms: Analysis of a Complex Dust Event in the Middle East, Submitted to Atmos. Meas. Tech., 2019.

Miller, S. D., C. C. Schmidt, T. J. Schmit, and D. W. Hillger: A case for natural colour imagery from geostationary satellites, and an approximation for the GOES-R ABI, Int. J. Rem. Sens., 33(13), 3999-4028, 2012.

Miller, S.D., and Turner R.E.: A Dynamic Lunar Spectral Irradiance Data Set for NPOESS/VIIRS Day/Night Band Nighttime Environmental Applications, IEEE Trans. Geosci. Remote Sens., 47(7), 2316-2329, doi:10.1109/TGRS.2009.2012696, 2009.

Piskozub, J. and McKee, D.: Effective scattering phase functions for the multiple scattering regime. Optics express. 19. 4786-94, doi:10.1364/OE.19.004786, 2011.

Polkinghorne R., and Vukicevic T.: Data Assimilation of Cloud-Affected Radiances in a Cloud-Resolving Model. Monthly Weather Review. 139. 755-773, doi: 10.1175/2010MWR3360.1, 2011.

Schmit, T. L., Griffith P., Gunshor M.M., Daniels J.M., Goodman S.J., and Lebair W.J.: A closer look at the ABI on the GOES-R series. Bull. Amer. Meteor. Soc., 98, 681-698, doi: https://doi.org/10.1175/bams-d-15-00230.1, 2017.

Skamarock, W. C., J. B. Klemp, J. Dudhia, D. O. Gill, D. M. Barker, M. G Duda, X.-Y. Huang, W. Wang, and J. G. Powers, 2008: A Description of the Advanced Research WRF Version 3. NCAR Tech. Note NCAR/TN-475+STR, 113 pp., doi:10.5065/D68S4MVH, 2008.

Smith T., and Guild J.: The C.I.E. colorimetric standards and their use. Trans. Opt. Soc. 33 73, 1931.

Stensrud D. et al.: Progress and challenges with Warn-on-Forecast. Atmospheric Research. 123. 2-16. 10.1016/j. Atmosres.2012.04.004, 2013.

Stephens G.L.: Radiation Profiles in Extended Water Clouds. II: Parameterization Schemes Journal of the Atmospheric Sciences November 1978, 35, (11), 1978.

Stockli R. et al.: The Blue Marble Next Generation—A true color Earth dataset including seasonal dynamics from MODIS, Nasa Earth Observatory, 2005.

Toth, Z., Albers S., and Xie Y.: Multiscale Data Assimilation and Forecasting. Bull. Amer. Meteor. Soc.,95 (2). ES30-ES33, doi: https://doi.org/10.1175/bams-d-13-00088.1, 2014.

Toth, Z., Buizza R.: Weather Forecasting: What Sets the Forecast Skill Horizon? In: The Gap Between Weather and Climate Forecasting: Subseasonal to Seasonal Prediction, 17-45. Eds.: A. Robinson and F. Vitard. Elsevier, 978-0-12-811714-9, doi: https://doi.org/10.1016/b978-0-12-811714-9.00002-4, 2019.

Veikherman D., Aides A., Schechner Y.Y., and Levis, A.: Clouds in The Cloud. Proc. ACCV, 659-674, doi: https://doi.org/10.1007/978-3-319-16817-3_43, 2014.

Vukicevic T. et al.: Mesoscale Cloud State Estimation from Visible and Infrared Satellite Radiances. Monthly Weather Review. 132. 10.1175/MWR2837.1, 2004.

Zhou J. et al.: A Fast Inverse Algorithm Based on the Multigrid Technique for Cloud Tomography. Journal of Atmospheric and Oceanic Technology. 31. 1653-1662, doi: 10.1175/JTECH-D-13-00184.1, 2014.

¶

¶

Ray Tracing Techniques compared among RTMs

	SWIm	CRTM (current version)	RRTMG	SHDOM	Monte Carlo
3-D Radiation (including sideways between columns)	Y	N	N	Y	Y
Multiple Scattering	Approximate	Y	Y	Y	Y
Fast Running	Y	Y	Y	N	N
Ground- air- or space-based observer	All	Space	Space	All	All
Curved Earth Shadow / Twilight	Y	N	N		Y
Moon/Stars/City Lights	Y	N	N		
2-D (directional) images	Y	Y	TOA SW up (Isotropic)	Y	Y
Wavelengths	VIS	VIS + IR	VIS + IR		
Grid Resolutions	All	All	All	<=100m	All

Gold Standard

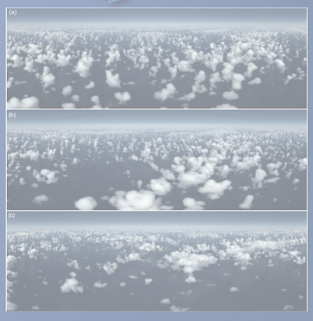

(Klinger, Mayer et al., 2017)

¶

¶

~~Figure 2.1. Overview showing features of interest for a sampling of radiative transfer packages.~~ ¶

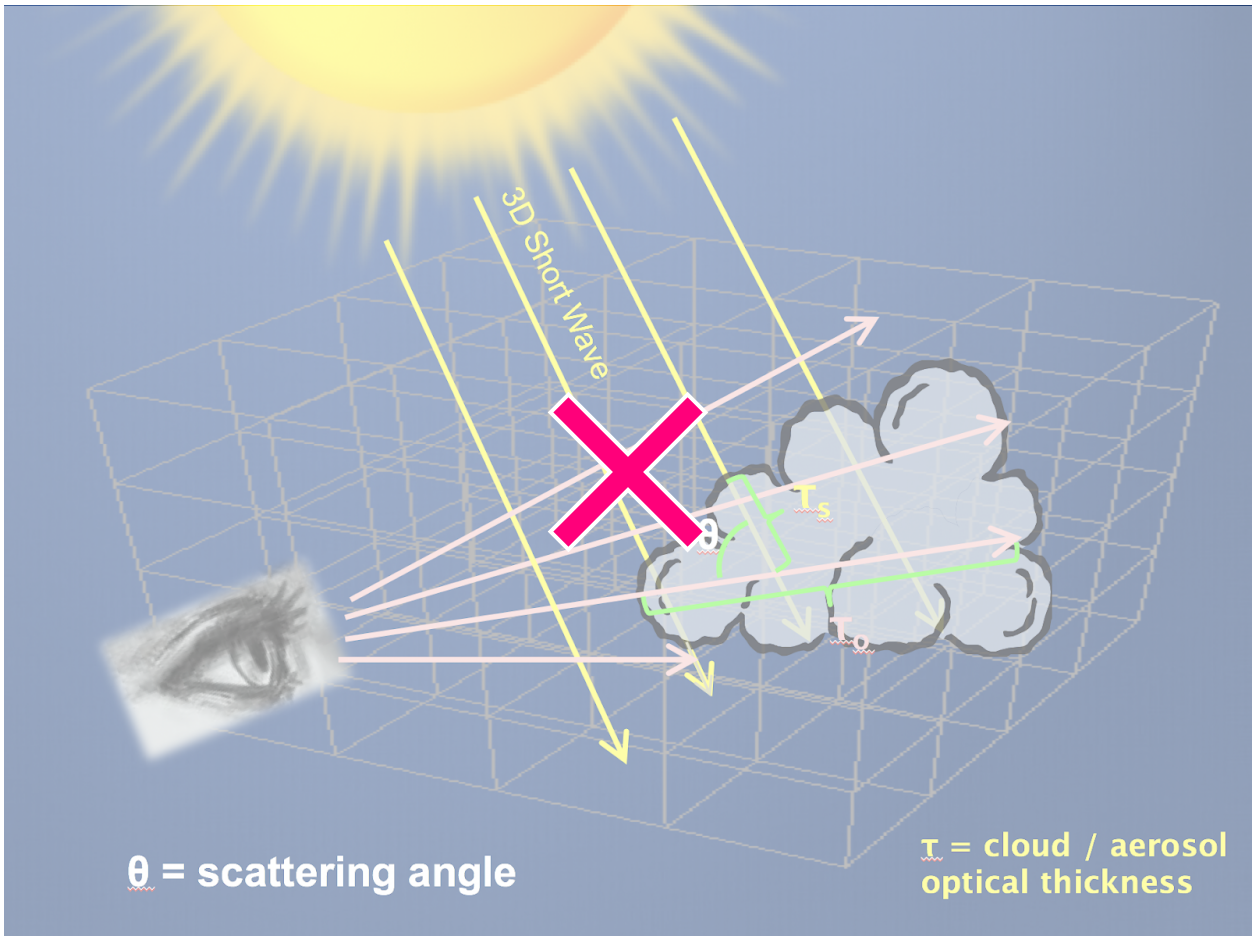
3D Short Wave
θ
T_s
T_o
θ = scattering angle
τ = cloud / aerosol optical thickness

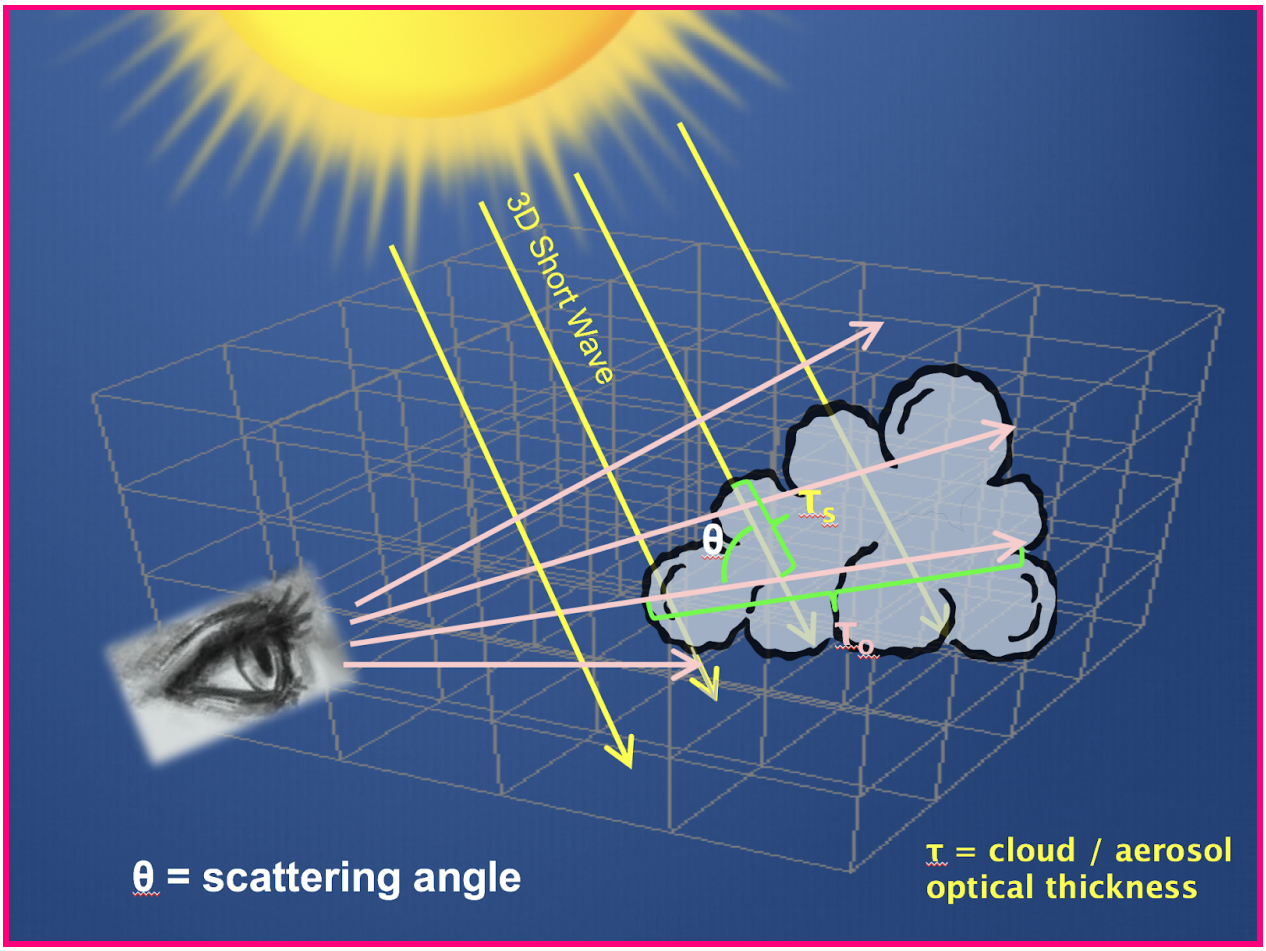

Figure ~~3.~~11. General ray-tracing procedure showing forward light rays (yellow) coming from the light source. A second set of light rays (pink) are traced backward from the observer. The forward and backward optical thicknesses (τ_s and τ_o) are calculated along these lines of sight and used for subsequent calculations to estimate the radiance on an angular grid as seen by the observer.

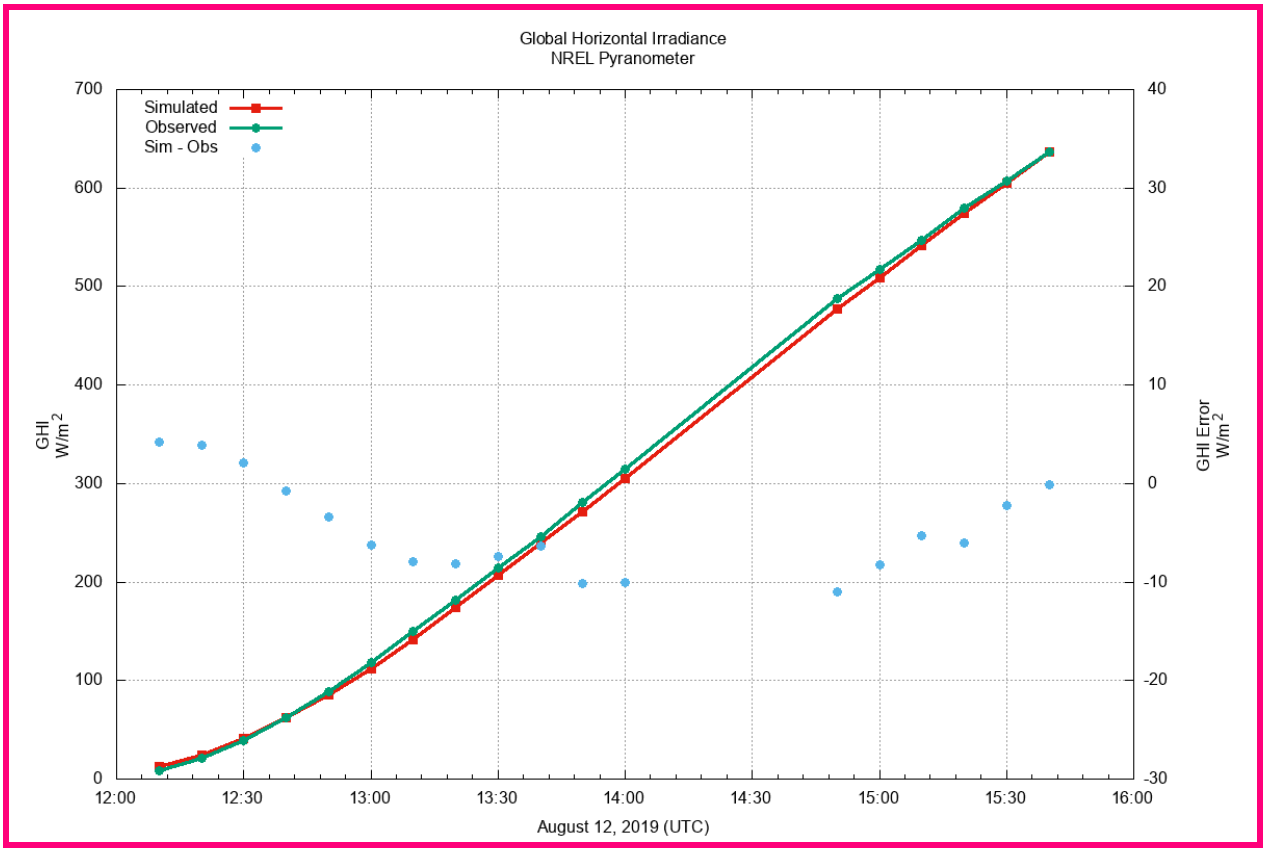

Figure 2. Time series of GHI values integrated from SWIm radiance images (red lines, vertical axis on left) compared with concurrent pyranometer observations in Wm^{-2} at NREL (green lines). The comparison spans a 4 hour period on the morning of August 12, 2019. Simulated minus pyranometer GHI values are plotted as blue circles (vertical axis on right). Sky conditions were free of significant clouds, with aerosol optical depth < 0.1.

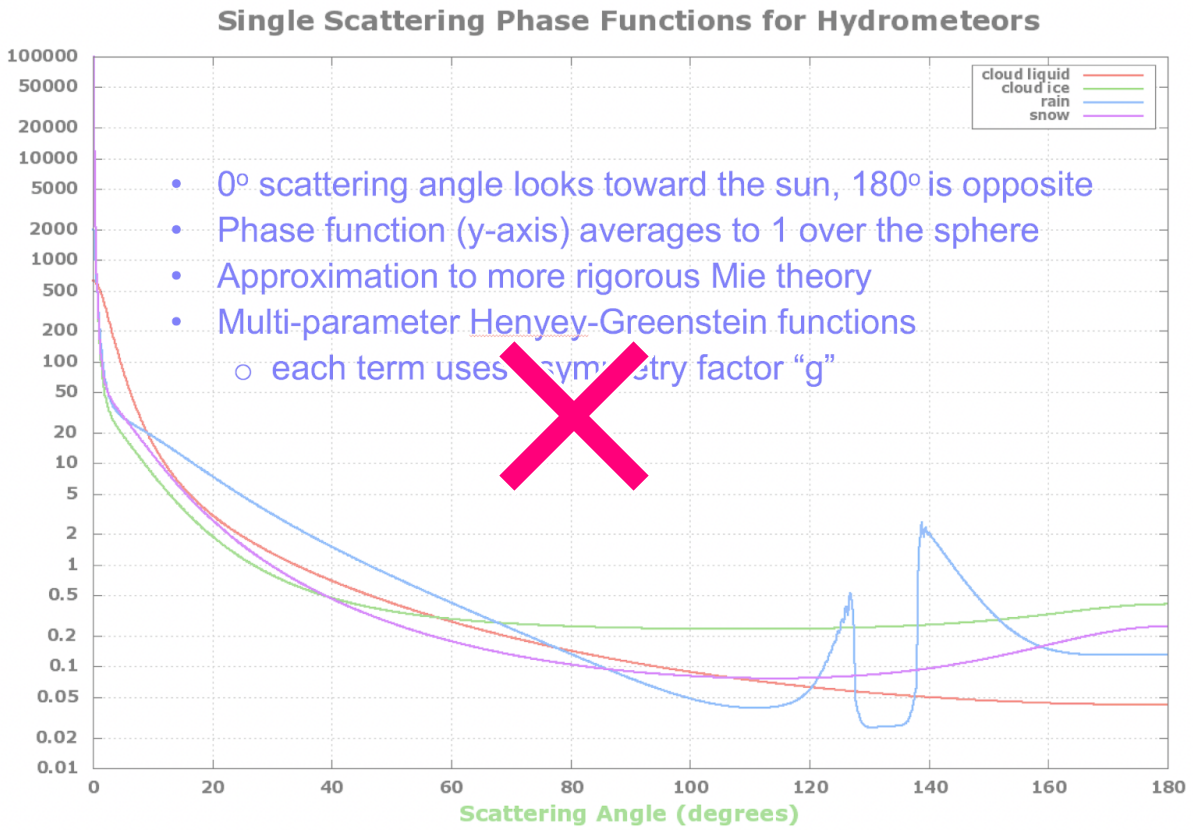
Single Scattering Phase Functions for Hydrometeors
cloud liquid
cloud ice
rain
snow
• 0° scattering angle looks toward the sun, 180° is opposite
• Phase function (y-axis) averages to 1 over the sphere
• Approximation to more rigorous Mie theory
• Multi-parameter Henyey-Greenstein functions
○ each term uses asymmetry factor "g"
100000
50000
20000
10000
5000
2000
1000
500
200
100
50
20
10
5
2
1
0.5
0.2
0.1
0.05
0.02
0.01
0
20
40
60
80
100
120
140
160
180
Scattering Angle (degrees)

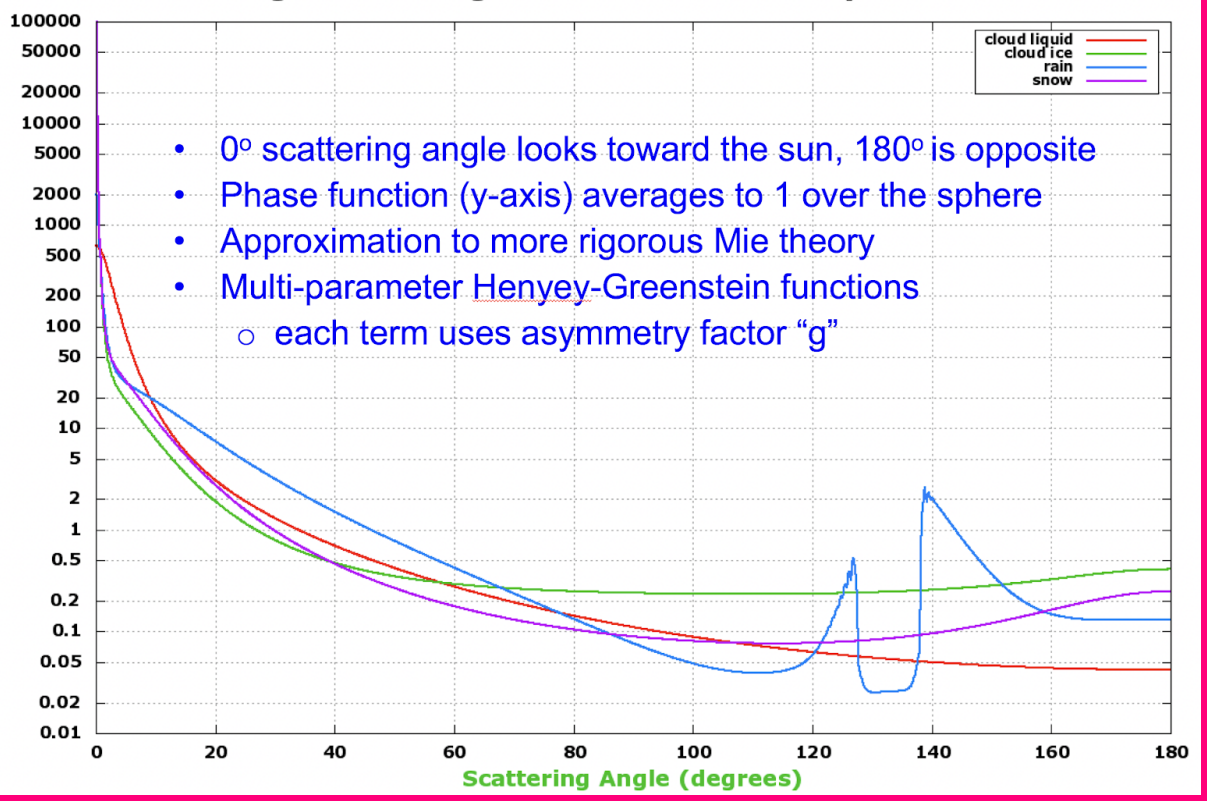
Single Scattering Phase Functions for Hydrometeors
cloud liquid
cloud ice
rain
snow
• 0° scattering angle looks toward the sun, 180° is opposite
• Phase function (y-axis) averages to 1 over the sphere
• Approximation to more rigorous Mie theory
• Multi-parameter Henyey-Greenstein functions
○ each term uses asymmetry factor "g"
100000
50000
20000
10000
5000
2000
1000
500
200
100
50
20
10
5
2
1
0.5
0.2
0.1
0.05
0.02
0.01
0
20
40
60
80
100
120
140
160
180
Scattering Angle (degrees)

Figure ~~3.2~~3. Single scattering phase functions used for cloud liquid, cloud ice, rain, and snow.

Aerosol Phase Functions

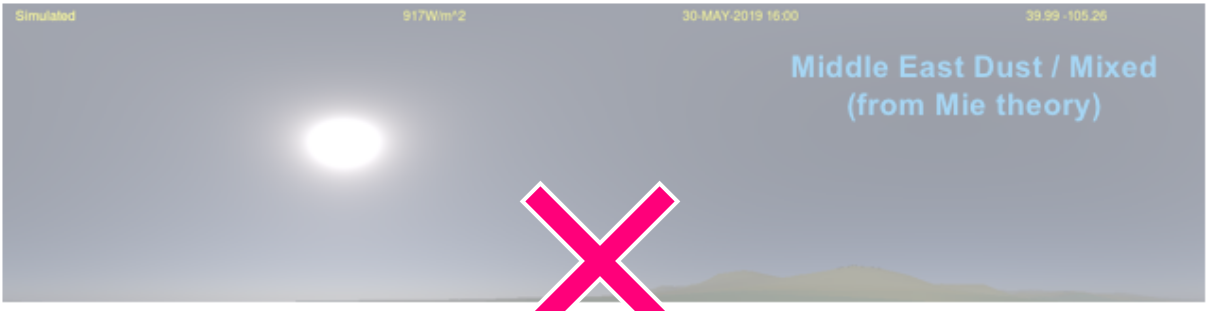

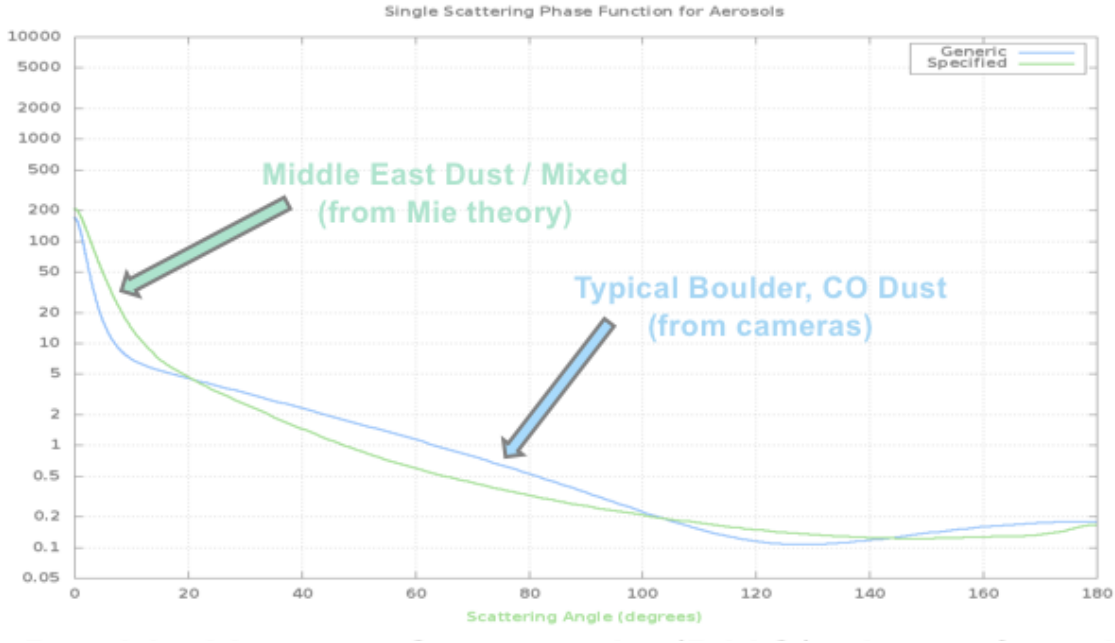

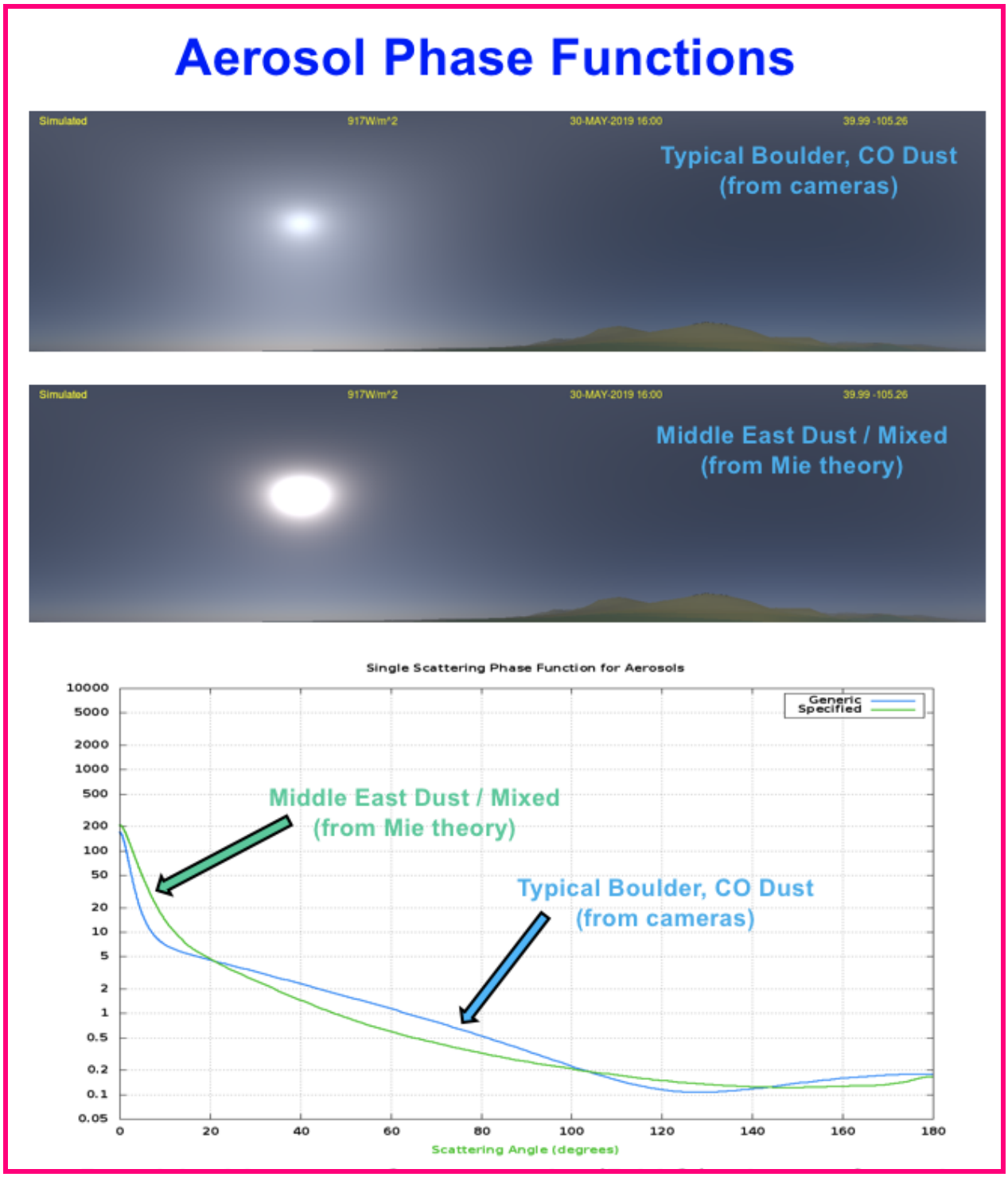

Figure ~~3.3~~4. Simulated panoramic images with an AOD of 0.1 using the Colorado empirical phase function (a), and the Mie theory mixed dust case (b). These two phase functions are compared in (c).

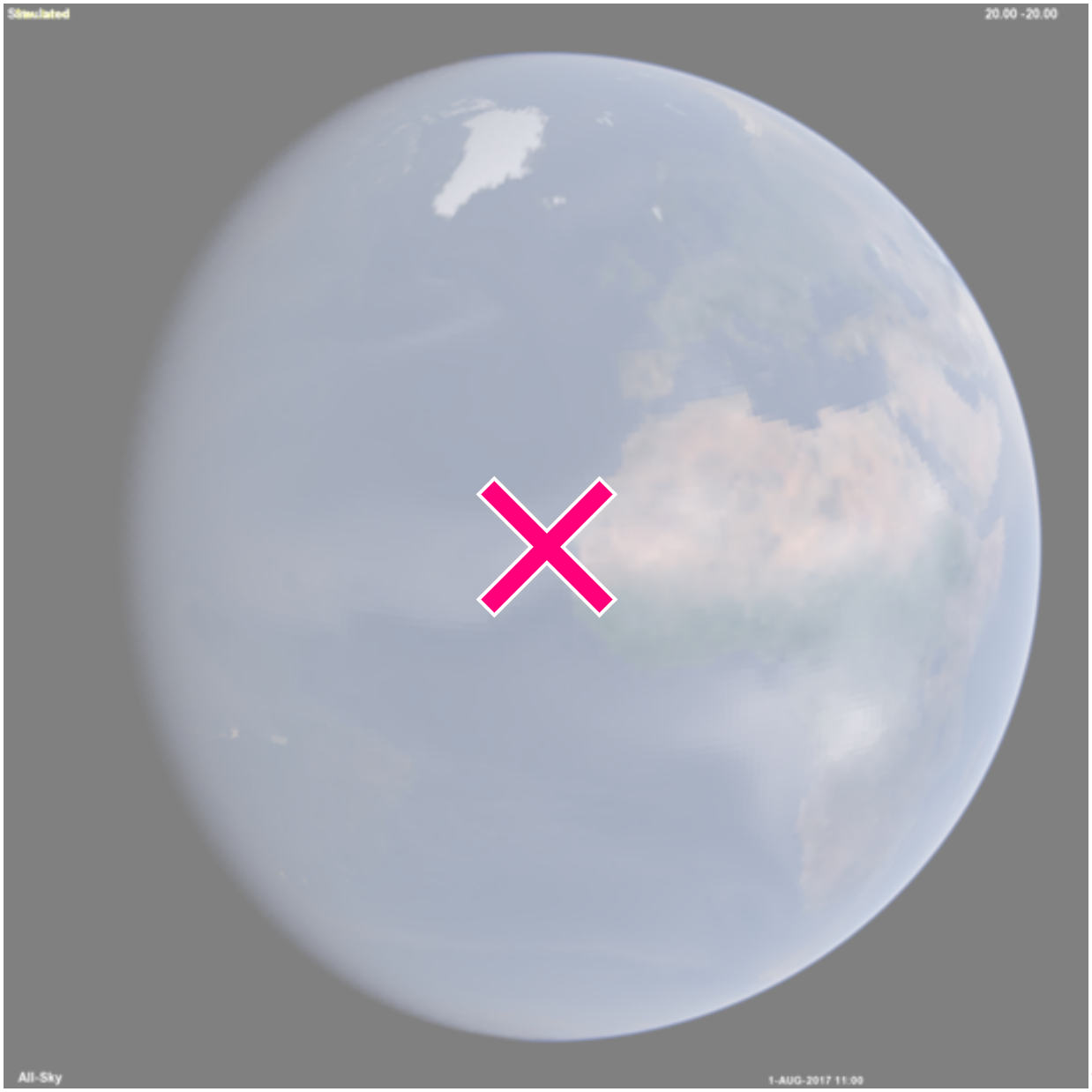

Figure 3.4. View from space of the NAVGEM global model, using aerosols only. The perspective point is $1.5 \times 10^6 km$ distant.

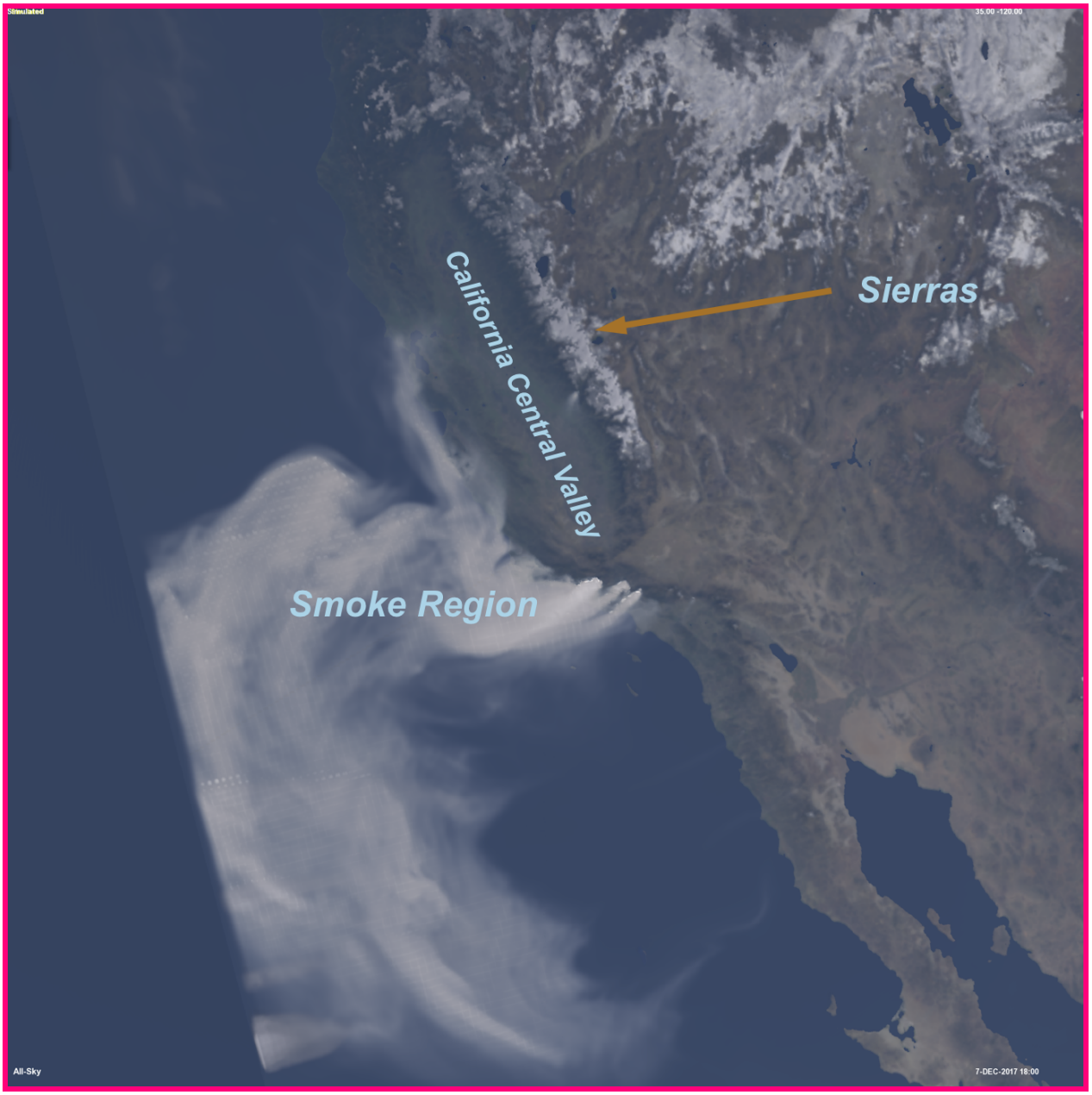

Figure ~~3.5~~5. Simulated image of a HRRR-Smoke forecast ~~showing the~~with a smoke plume from ~~California wildfires during December 2017~~the December 2017 California wildfires. The view is zoomed in from a perspective point at $40000\ km$ altitude.

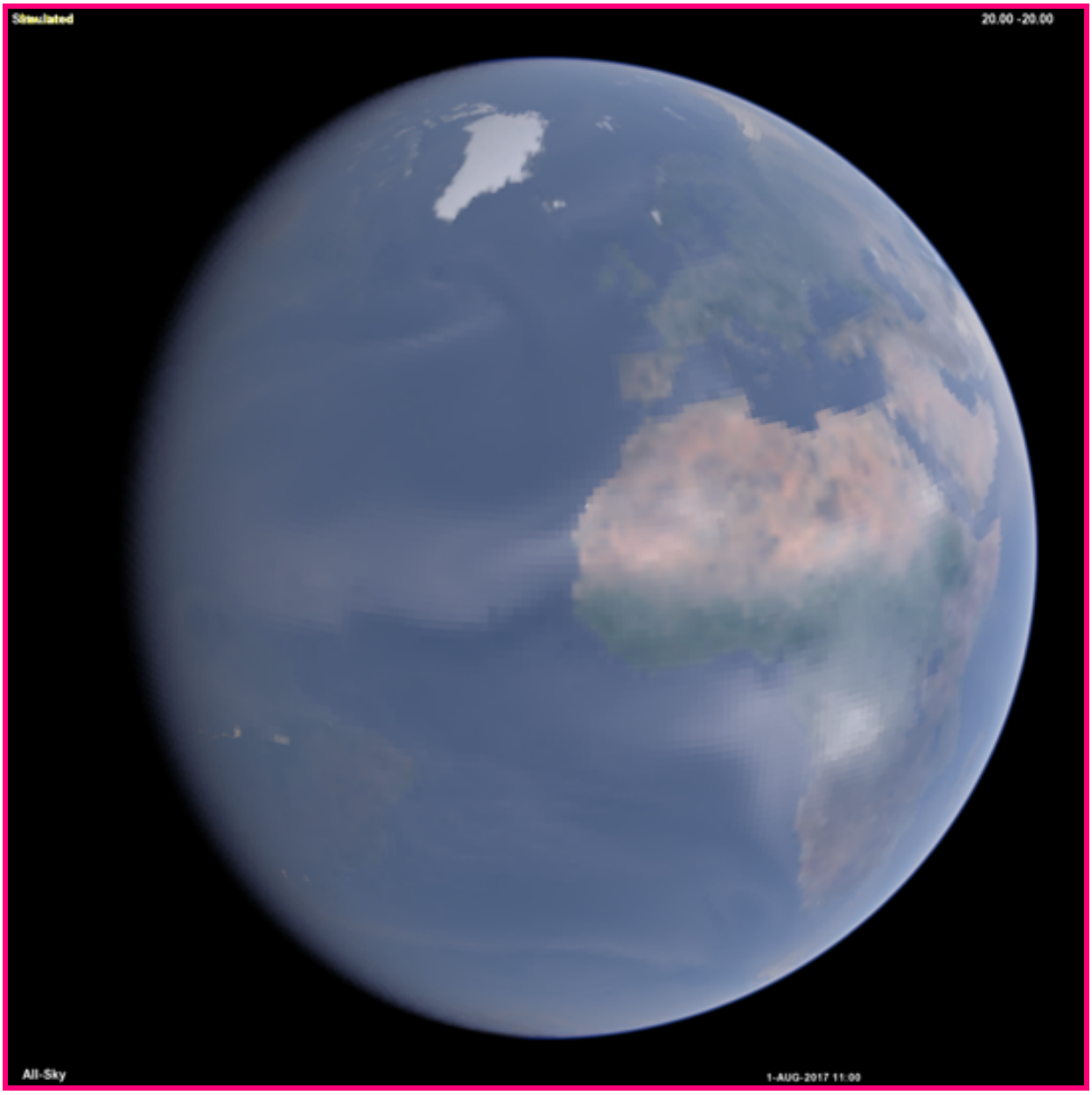
Simulated
20.00 -20.00
All-Sky
1-AUG-2017 11:00

Figure ~~3.66~~. View from space of the NAVGEM global model, using aerosols only. The perspective point is $1.5 \times 10^6 km$ distant.

Figure 7. In-situ panoramic view in the lower troposphere showing smoke aerosols and hydrometeors. This is part of an animation simulating an airplane landing at the Denver International Airport. The panorama spans 360^o from a perspective $\sim 4km$ above ground. Hydrometeor fields are from a LAPS analysis.

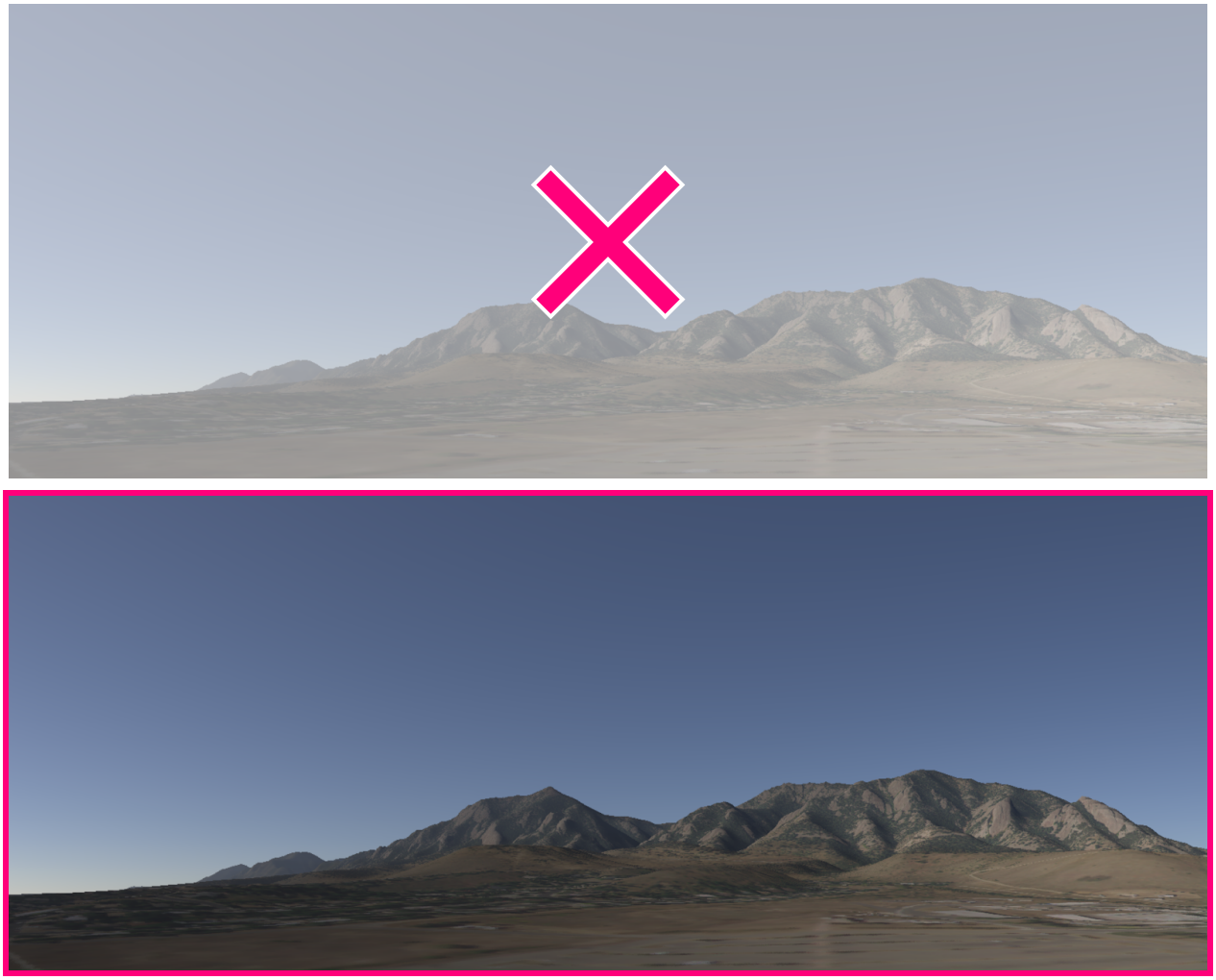

Figure ~~3.7~~8. SWIm generated image for a hypothetical clear-sky case having ~~a small amount of aerosols~~an aerosol optical depth ~0.05. The model grid and associated terrain data is at 30m resolution and surface spectral albedo information is derived from 0.7m resolution aerial imagery from the USDA. The vantage point is from the U.S. Department of Commerce campus in Boulder, Colorado, looking at azimuths from south through west.


Simulated
East
1213W/m^2
South
5-AUG-2017 10:00
West
24.70N 51.50E 4000m

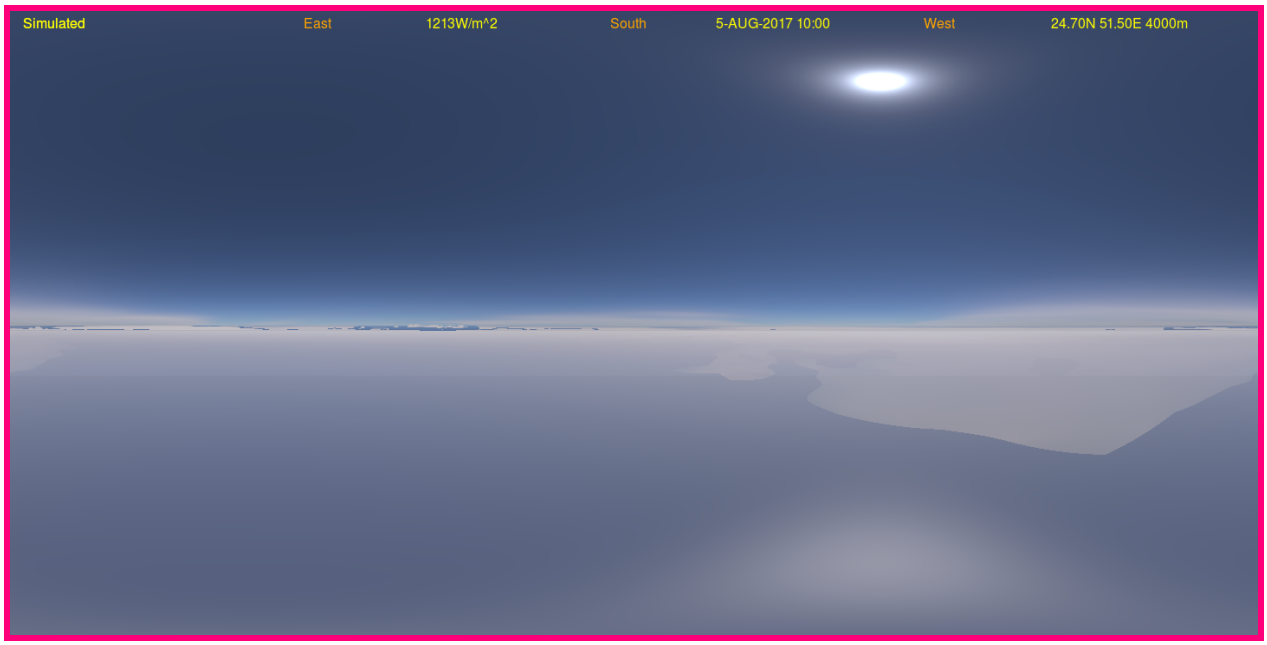
Simulated
East
1213W/m^2
South
5-AUG-2017 10:00
West
24.70N 51.50E 4000m

¶

Figure ~~4.1~~9. View ~~(a)~~ from ~~4 km~~ $4km\ (a)\ and\ 20m$ (b) above the Persian Gulf of a RAMS model simulation showing dust, hydrometeors, land surface, and water including sun glint, displayed with a cylindrical (panoramic) projection. ~~The vantage point in (b) is 20 m above the water surface.~~

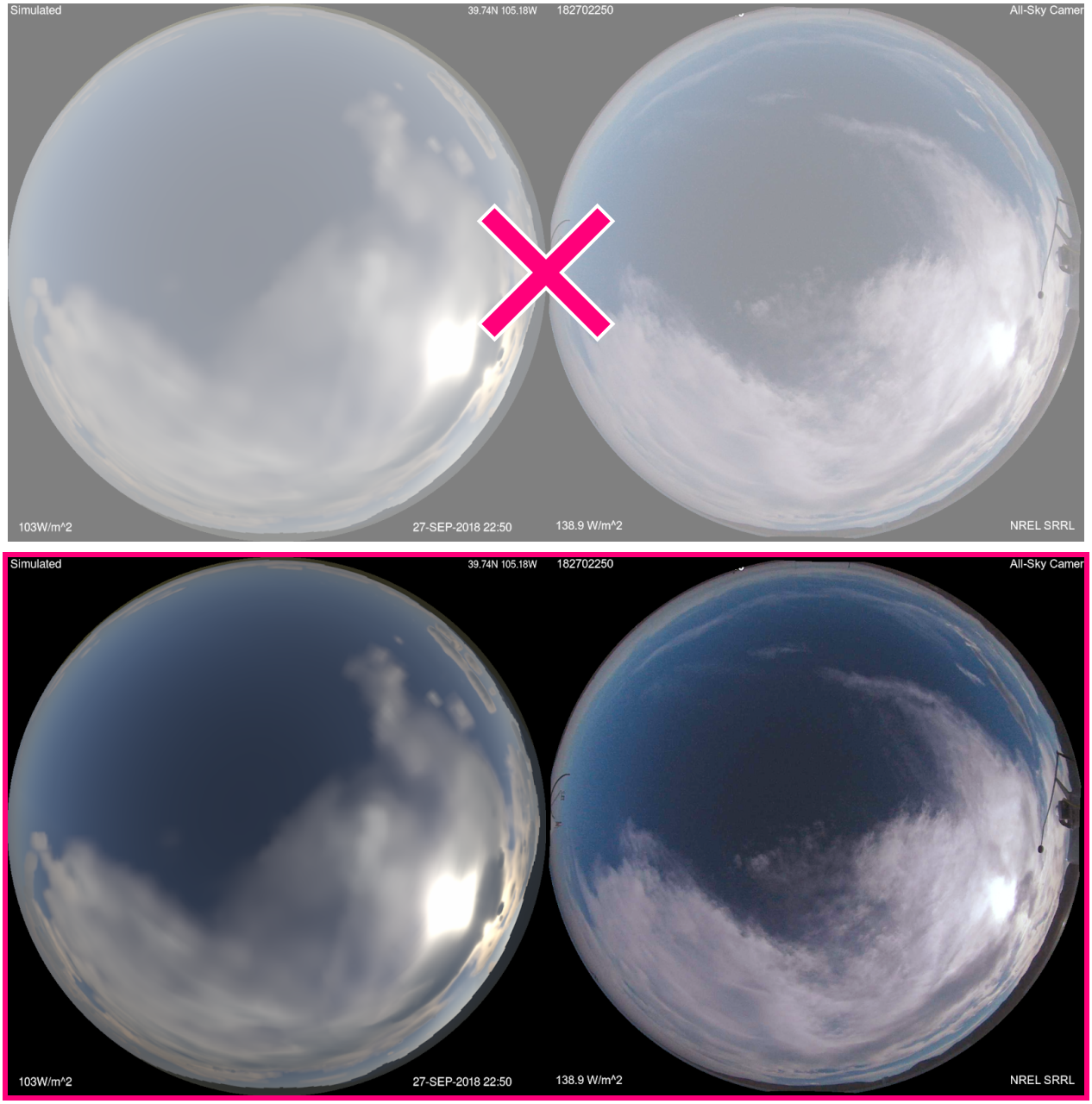

Figure ~~4.2~~10. Comparison of observed ~~allsky image~~ (right) to simulated (left) ~~over Golden, Colorado on September 27, 2018 at 2250UTC. This ground-based all-sky view is on a polar equidistant projection showing the upward looking hemisphere.~~ polar equidistant projection images showing the upward looking hemisphere from a ground-based location in Golden, Colorado on September 27, 2018 at 2250UTC. LAPS analysis fields are used for the simulated images.

Figure ~~4.3~~11. A comparison of aerosols at 2100UTC on August 20, 2018 in Golden, Colorado showing ~~the simulated panoramic image~~ a panoramic simulated (top) and an all-sky camera image (bottom). The correlation $\bar{r}$ between the images is denoted as 0.961.

Figure ~~4.4~~12. Side-by-side comparison ~~(SWIm image on the left, DSCOVR-EPIC image on the right). Both images are from approximately 1800UTC on April 28, 2019~~.

of global cloud coverage viewed from space at approximately 1800UTC on April 28, 2019 as provided by DSCOVR-EPIC (camera observed image, right), and analyzed by LAPS (21 km horizontal resolution) and visualized by SWIm (simulated image, left).

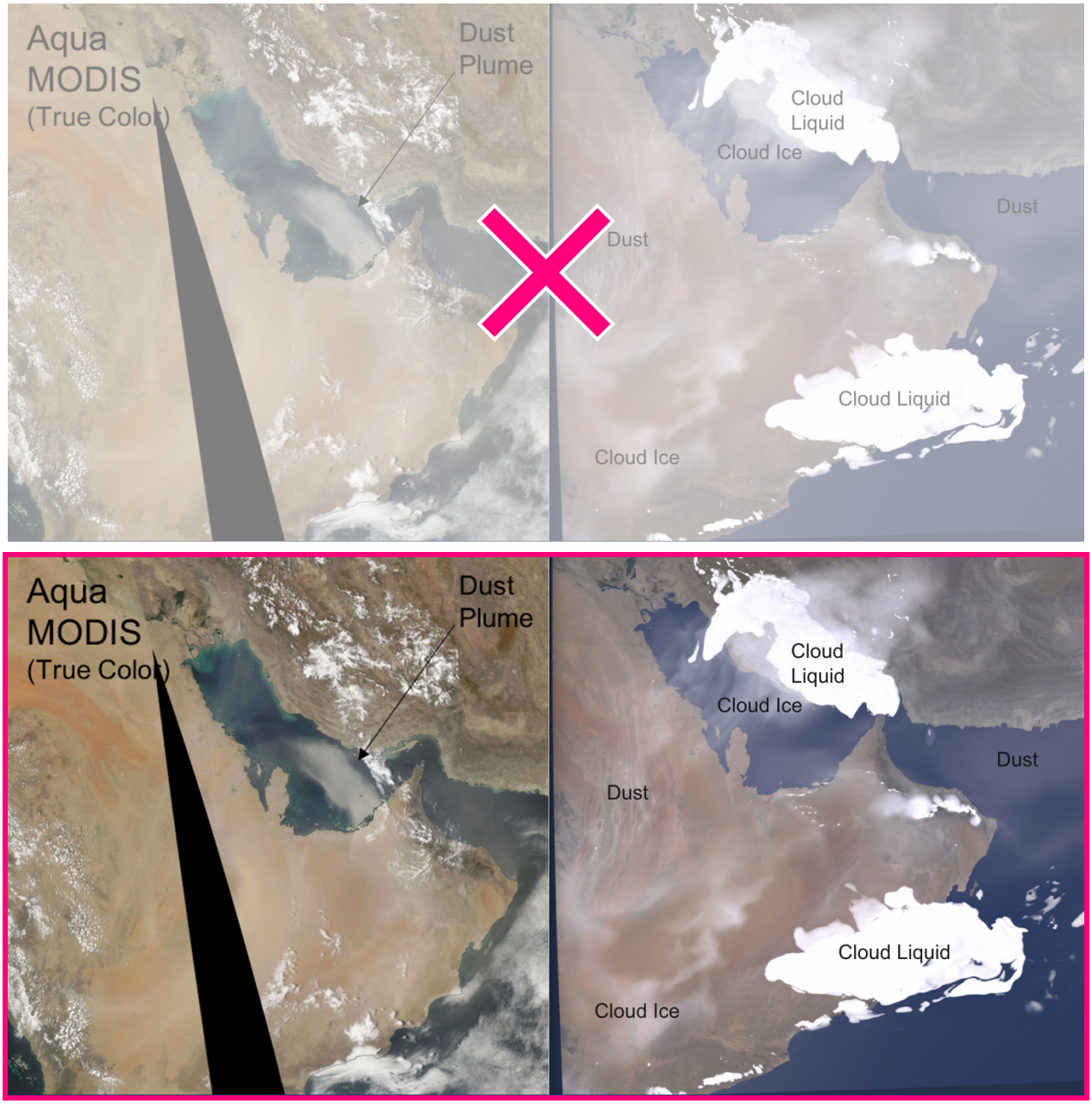

Figure ~~4.5~~13. Aqua-MODIS image (left) taken from passes at about 1330 local time over the Arabian Peninsula compared with SWIm visualization of a RAMS model forecast (right) from 1000UTC. Areas having predominantly dust, cloud liquid, and cloud ice are annotated in the images.

Figure 14. SWim image from a 3D LAPS cloud analysis using satellite data without camera input (a), is shown with a camera image (b), and the SWIm image using 3D clouds modified via a color ratio algorithm (c). The NREL camera image is from May 24, 2019 at 2240UTC.

	SWIm	CRTM	RRTMG	SHDOM	Monte Carlo
3-D Radiation (including sideways) between columns	Yes	No	No	Yes	Yes
Multiple Scattering	Approximate	Yes	Yes	Yes	Yes
Fast Running	Yes	Yes	Yes	No	No
Ground- air- or space-based observer	All	Space	Space	All	All
Curved Earth Shadow / Twilight	Yes	No	No		Yes
Moon / Stars / City Lights	Yes	No	No		
2-D (Directional) Images	Yes	Yes	TOA SW up (Isotropic)	Yes	Yes
Wavelengths	Visible	Vis + IR	Vis + IR		
Grid Resolutions	All	All	All	$\leq 100m$	All

Table 1. Overview of functionality in a sampling of radiative transfer packages.

Step 1a: Forward rays from dominant light source (in 3-D grid, including hydrometeors and aerosols)
Step 1b: Backward rays from observer (in 3-D grid, including hydrometeors and aerosols)
Step 2: Rays from Sun and from observer (in clear air, extending beyond model grid)
Step 3: Combination of radiance components, generation of RGB image display.

Table 2. List of ray tracing steps used in SWIm. Steps 1a and 1b are illustrated in Fig. 1.

Case	g_1	g_2	f_c	f_b	ω
Colorado Dust	.59, .60, .61	.895, .900, .905	.12, .12, .12	.550, .550, .550	.935, .92, .86
Saudi Arabian Mixed Dust and Pollution	.23, .27, .29	.915, .925, .933	.58, .54, .53	.562, .558, .558	.96, .96, .96

Table 3. Two cases showing the four fitted phase function parameters g_1 , g_2, f_c, and f_b as well as single scattering albedo ω, for each of the three reference wavelengths, 615nm, 546nm and 450nm.

Quantity being assessed	Measurements	Methodology	Outcome / Result	Comments
GHI	NREL pyranometer	546nm horizontal spectral radiance integrated over sky dome, converted to global horizontal irradiance.	Typically within $10-20\ \frac{W}{m^2}$ in cloud-free skies. SWIm ~50% too high in uniform overcast.	Sensitive to both SWIm raytracing, and cloud/aerosol analysis.
Spatially (radially) distributed spectral radiance (converted to RGB images) from surface vantage point	NREL all-sky camera	Correlation ($\bar{r}$) (described in text) calculated over sky dome between concurrent SWIm and camera RGB images.	Typically 0.90 to 0.98 in cloud-free areas (where aerosols remain important) and ~0.50 with significant cloud cover.	Higher scores contingent on masking 12 degree radius around sun affected by camera glare. Cloudy results strongly affected by quality of cloud (and to lesser degree, aerosol) analysis, and thus highly variable; in best cases, correlation reaches ~0.8.
Spatially distributed images from space	DSCOVR EPIC RGB images and red band reflectance factor data	Subjective comparison of SWIm and concurrent DSCOVR/EPIC data	Reflectance factor distribution matches anticipated values from 5% in darkest clear oceanic areas to ~1.1 in bright tropical convection.	Results sensitive to analysis quality of clouds (and aerosols), whose locations are well captured both on large and small scales.

~~Appendix A~~Table 4. List of SWIm validation methods being developed.

Appendix A. Aerosol optical properties for Arabian peninsula case.

The Arabian Peninsula case is calculated using the representative dust model derived as follows from the Capo Verde site in the AERONET network (Holben et al., 1998). We the applied EPA positive matrix factorization (PMF) 5.0 model (available at https://www.epa.gov/air-research/positive-matrix-factorization-model-environmental-data-analyses) to the dataset, using as factors the aerosol optical depth (AOD) for the fine and coarse modes and the total absorption aerosol optical depth (AAOD) from the Capo Verde site, for all Level 2.0 Inversion V3 data from 1994-2017. Two factors were derived (Figure ~~1~~A1). The factor with high AOD contributions from the coarse mode was flagged as the dust source. The derived absorption angstrom exponent (AAE) for Factor 1 was 4.387 for the Capo Verde site and the average extinction Ångstrom exponent (EAE) was 0.0905, lying in the range of the dust aerosol characteristics identified in Giles et al. (2012). The factor with high AAOD was believed to be associated with urban / industrial aerosols. For those samples, the averaged AAE and EAE were 0.729 and 1.164, respectively, similar to reported optical properties of absorbing fine particles (Giles et al., 2012). We selected data with corresponding PMF-identified dust source contributions larger than 95% to characterize the dust properties. The average normalized volume size distributions for the dusty days is shown in Figure ~~2~~A2. We used the average retrieved refractive index for the same dusty days, and the aspect ratio distribution in Dubovik et al (2006), to calculate the phase function and related optical properties used in this study.

Figure ~~1~~A1. Optical source profile (% of species in each source) for the Capo Verde dataset.

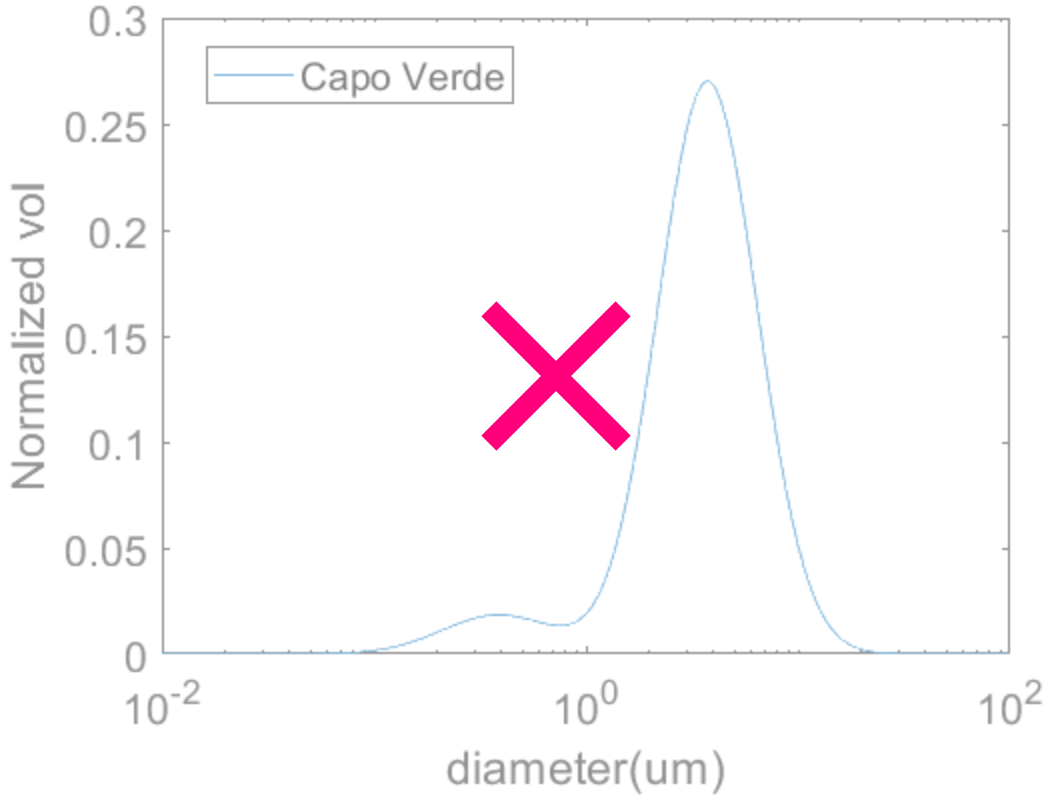
Capo Verde
Normalized vol
0.3
0.25
0.2
0.15
0.1
0.05
0
10^{-2}
10^{0}
10^{2}
diameter(um)

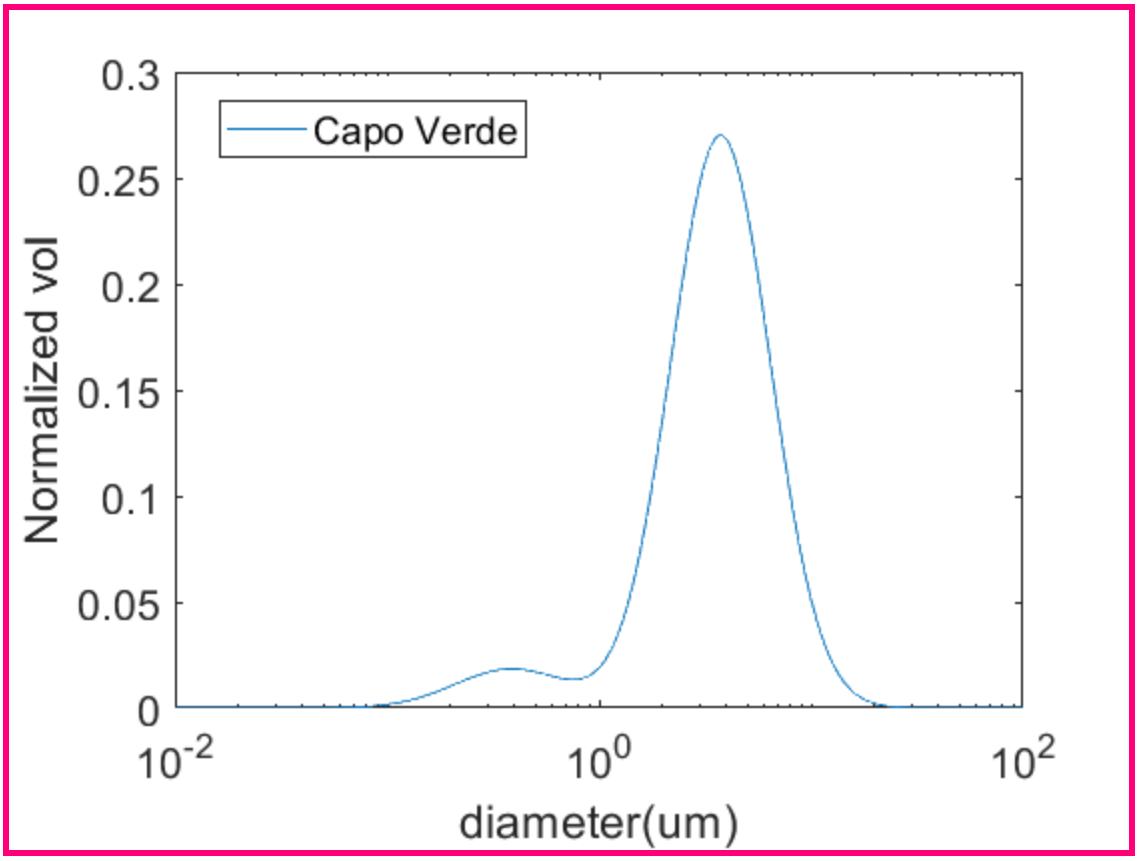
Capo Verde
Normalized vol
0.3
0.25
0.2
0.15
0.1
0.05
0
10^{-2}
10^{0}
10^{2}
diameter(um)

Figure ~~2~~A2. Average normalized volume size distribution for dust-dominated days in the Capo Verde data set.

Appendix B. Multiple scattering effective phase functions for additional species.

For multiple scattering for hydrometeors beyond cloud liquid we follow a procedure similar to that described in section 3.4.2 with these primary differences. For the rain phase function we specify via eq. 13 a parameterization for multiple scattering. The optically thin rain component is given here:

$$P_{thin}(\theta,\lambda) = 0.1\, p(\theta, 0.99^{\tau_o}) + 1.05\, p(\theta, 0.75^{\tau_o}) - 0.35\, p(\theta, 0.0) + 0.20\, p(\theta, -0.2) \quad \text{(B1)}$$

If there is a mixture of cloud liquid and rain then we interpolate between the results of eqs. 18 and B1.

For cloud ice, the optically thin component is given by.

$$P_{thin}(\theta,\lambda) = 0.50\, p(\theta, 0.999^{\tau_o}) + 0.71\, p(\theta, 0.991^{\tau_o}) - 0.25\, p(\theta, 0.0) + 0.04\, p(\theta, -0.2) \quad \text{(B2)}$$

For snow eq. B3 is used. If there is a mixture of cloud ice and snow then we interpolate between the results of eqs. B2 and B3.

$$P_{thin}(\theta,\lambda) = 0.50\, p(\theta, 0.999^{\tau_o}) + 0.45\, p(\theta, 0.991^{\tau_o}) + 0.03\, p(\theta, 0.0) + 0.02\, p(\theta, -0.2) \quad \text{(B3)}$$